Palaeogeography, Palaeoclimatology, Palaeoecology 301 (2011) 1–17

Contents lists available at ScienceDirect

Palaeogeography, Palaeoclimatology, Palaeoecology

journal homepage: www.elsevier.com/locate/palaeo

Pangean great lake paleoecology on the cusp of the end-Triassic extinction

Jessica H. Whiteside [a,*], Paul E. Olsen [b], Timothy I. Eglinton [c], Bruce Cornet [d], Nicholas G. McDonald [e], Philip Huber [f]

[a] Department of Geological Sciences, Brown University, Box 1846, Providence, RI 02912, USA
[b] Department of Earth and Environmental Sciences, Lamont-Doherty Earth Observatory of Columbia University, Palisades, NY 10964, USA
[c] Department of Marine Geology and Geophysics, Woods Hole Oceanographic Institution, Woods Hole, MA 02543, USA
[d] 16921 Cielito Lindo Dr., El Paso, TX 79938, USA
[e] Westminster School, Simsbury, CT 06070, USA
[f] Geoscience Books, PO Box 1036, Faribault, MN 55021, USA

ARTICLE INFO

Article history:
Received 1 September 2009
Received in revised form 9 November 2010
Accepted 25 November 2010
Available online 3 December 2010

Keywords:
Central Atlantic magmatic province
End-Triassic extinction
Paleolimnology
Species flocks
Carbon isotopes
Semionotidae
Redfieldiidae

ABSTRACT

Triassic and Early Jurassic age lacustrine deposits of eastern North American rift basins preserve a spectacular record of precession-related Milankovitch forcing in the Pangean tropics in the wake of the end-Triassic extinction event (ETE). The abundant and well-preserved fossil fish assemblages from these great lakes show cyclical changes that track the permeating hierarchy of climatic cycles. To detail ecosystem processes correlating with succession of fish communities, bulk $\delta^{13}C$ was measured through a 100 ky series of precession-forced lake level cycles in the lower Shuttle Meadow Formation of the Hartford rift basin, Connecticut, that were deposited within 50 ky after the ETE. The deep-water phase of one of these cycles, the Bluff Head Bed, has produced thousands of articulated fish. There are fluctuations in the bulk $\delta^{13}C_{org}$ in the cyclical strata that reflect differing degrees of lake water stratification, nutrient levels, and relative proportion of algal vs. plant derived organic matter that trace fish community changes. Extrinsic changes in the global exchangeable reservoirs can be excluded as an origin of this variability because compound-specific $\delta^{13}C$ of *n*-alkanes from plant leaf waxes in the same strata show no such variability. Although higher taxonomic levels of the fish communities responded largely by sorting of taxa by environmental forcing, at the species level the holostean genus *Semionotus* responded by in situ evolution, and ultimately extinction, of a species flock. Fluctuations at the higher frequency, climatic precessional scale are mirrored at lower frequency, eccentricity modulated scales, all following the lake-level hierarchical pattern. Thus, changes in lacustrine isotopic ratios amplify the Milankovitch climate signal that was already intensified by sequelae of the end-Triassic extinctions. The degree to which the ecological structure of modern lakes responds to similar environmental cyclicity is largely unknown, but similar patterns and processes are present within the Neogene history of the East African great lakes.

1. Introduction

The end-Triassic extinction event (ETE) marks one of the largest mass-extinctions of the Phanerozoic (Benton, 1995) and the global rise to ecological dominance of dinosaurs (Olsen et al., 2002). The causes of this mass-extinction have been hotly debated, with recent discussion focusing on the role of the emplacement of the giant Central Atlantic Magmatic province (CAMP), which began erupting at the onset of the mass extinction event and extruded basalt over an area of <10 million km^2 (Marzoli et al., 1999, 2004). The CAMP eruptions seem to be related to the rifting of Pangea that led to the opening of the Atlantic Ocean, and may represent the onset of the formation of the oldest Atlantic oceanic crust (Olsen et al., 2003a). Rifting began 32 million yr prior to the ~600 ky eruption of the CAMP at about 201.5 Ma (Schoene et al., 2006), and continued for at least a few million years afterward (Kent and Olsen, 2008), in the process forming a vast series of rift basins around the edges of what would become the Central Atlantic margin (Fig. 1). Many of these rifts contained lakes that in a modern context would be called great lakes because they are on a scale similar to the large rift lakes of East Africa, such as lakes Edward, Tanganyika, or Malawi (Fig. 2). The Triassic–Jurassic great lakes rose and fell in depth, often drying out entirely, producing lacustrine sedimentary cycles with frequencies characteristic of orbital forcing. Lacustrine sedimentation continued in many rifts throughout the entire duration of CAMP eruption and implacement, with practically no perceptible lags (Olsen, 1986, 2003a; Whiteside et al., 2007). In eastern North America, the oldest lava flows of the CAMP are capped by a series of distinctive lacustrine cycles produced by some of the largest of lakes in the basin (Whiteside et al., 2007). It now appears that both terrestrial and marine

* Corresponding author. Tel.: +1 401 863 6465; fax: +1 401 863 2058.
E-mail address: Jessica_Whiteside@Brown.edu (J.H. Whiteside).

0031-0182/$ – see front matter © 2010 Elsevier B.V. All rights reserved.
doi:10.1016/j.palaeo.2010.11.025

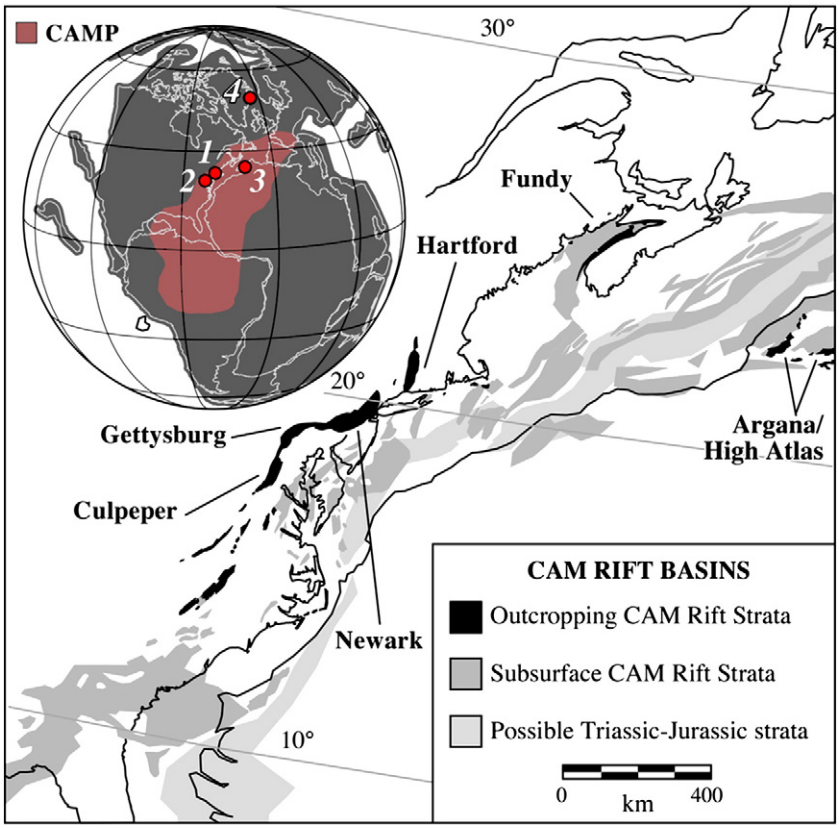

Fig. 1. Map of central Pangea showing distribution of Central Atlantic margin (CAM) rift basins mentioned in text with an inset showing the pre-erosional distribution of the CAMP with end-Triassic continental positions: 1, Hartford basin; 2, Newark, Gettysburg, and Culpeper basins, 3, Moroccan basins including the Argana and High Atlas basins; 4, Jamesonland basin, East Greenland. Inset based on map courtesy of Christopher Scotese and modified from Whiteside et al. (2010).

extinctions continued during the eruption of these initial CAMP lava flows (Whiteside et al., 2010), and into the time represented by these large lakes. This paper documents the paleoecology of a core sampling strata deposited by great lakes that rose and fell during this time of extinction and CAMP eruption, and focus on a microstratigraphic excavation in one of the lakebeds (the Bluff Head Bed: Fig. 3) in the Shuttle Meadow Formation of the Hartford rift basin of Connecticut and Massachusetts, USA.

The deep-water deposits of the Bluff Head Bed constitute a widespread Konzentrat Lagerstätte of fish and other fossils. Despite the fact that beautiful fish specimens from this famous deposit have been collected for over one and one half centuries (e.g., Redfield, 1841), this is the first detailed paleoenvironmental examination of these lake strata. This analysis elucidates how lacustrine ecosystems responded to lake depth driven by Milankovitch forced climate change during a time of extreme global stress caused by one of the largest magmatic events in Earth history.

2. Geological and chronostratigraphic context

The lacustrine strata described here formed largely during the Middle to Late Triassic in rift basins developed in a continental setting, along a huge central Pangean rift zone from East Greenland through the Gulf of Mexico (Fig. 1). The eastern North American section of these rift valleys, collectively termed the Newark Supergroup, filled with several kilometers of lacustrine, fluvial and igneous rocks along reactivated Paleozoic thrust faults that follow the grain of the Appalachian orogen. The Hartford basin is one of these rifts that formed along the western boundary of the rift system, and was at about 20° north latitude during the eruption of the CAMP (Kent and Tauxe, 2005). Despite the vast climate differences from the present (e.g. a lack of polar ice caps), a humid equatorial zone of modern dimensions existed (Kent and Tauxe, 2005; Olsen and Kent, 2000), and the Hartford basin lay at the transition between this zone and the arid belt.

The Hartford basin is a half-graben, bounded on its eastern side by a west-dipping border fault system. The ~5 km of syn-rift strata dip towards the border fault, and several kilometers of post-rift erosion has exposed the up-dip edges of nearly the entire section from Late Triassic to Early Jurassic in age (Fig. 3). The cores and outcrops examined here are from the Shuttle Meadow Formation, near the middle of the preserved basin fill. These sediments directly overlie the Talcott Formation, which is the oldest occurrence of CAMP lava and associated pyroclastics in the basin (Fig. 3); where these strata are absent, the Shuttle Meadow Formation rests directly above the New Haven Formation. At all known localities, the Shuttle Meadow Formation is overlain by the Holyoke Basalt, the thickest CAMP lava in the basin.

The stratigraphy of the Shuttle Meadow Formation is depicted in Fig. 4, following the stratigraphic nomenclature of Olsen et al. (2005) and Kent and Olsen (2008). The formation consists of a lower, strongly cyclical Durham Member and an overlying mostly red Cooks Gap Member with less obvious cyclicity. The Durham Member is the focus of study here because it is marked by a series of distinctive fish-bearing beds that comprise the deeper water portions of sedimentary cycles. The most fossiliferous and best known of these units is the Bluff Head Bed.

The numerical age of the Shuttle Meadow Formation is tightly constrained above and below by the Talcott and Holyoke basalts correlative to the North Mountain (Fundy basin) and Preakness (Newark basin) basalts, respectively, that have produced high-precision U–Pb ages (Schoene et al., 2010; Blackburn et al., 2009). Based on several lines of evidence, the underlying Talcott Formation is

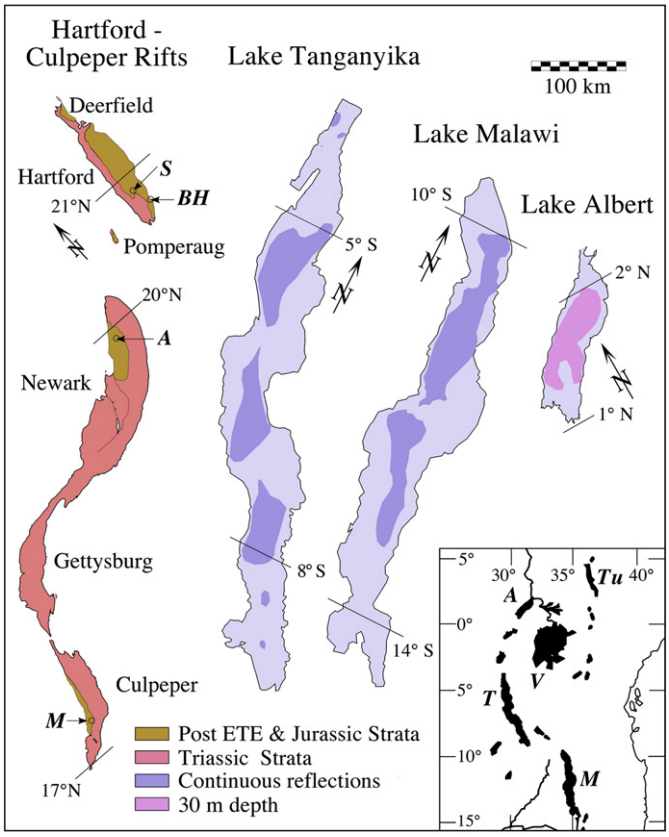

Fig. 2. Comparison to scale of North American Triassic–Jurassic great lakes and East African great lakes to the same scale. Paleolatitudes for Triassic–Jurassic great lakes shown (based on Kent and Tauxe, 2005). The areas with continuous reflections (darker blue) in Lakes Tanganyika and Malawi (based on Scholz and Rosenahl, 1988) refers to seismic reflection facies in strata likely to be preserved if these modern rifts were to be as deeply eroded as those in eastern North America. For Lake Albert, the topography below 30 m water depth flattens out and this is likely to be an area of sediments preserved after considerable erosion (based on Karner et al., 2000). A, ACE core sections of the lower Feltville Formation; BH, Bluff Head excavations; M, Midland outcrops of the lower Midland Formation; S, Silver Ridge cores. Inset showing distribution of the East African great lakes (based on Scholz and Rosenahl, 1988): A, Lake Albert; M, Lake Malawi; T, Lake Tanganyika; Tu, Lake Turkana; V, Lake Victoria.

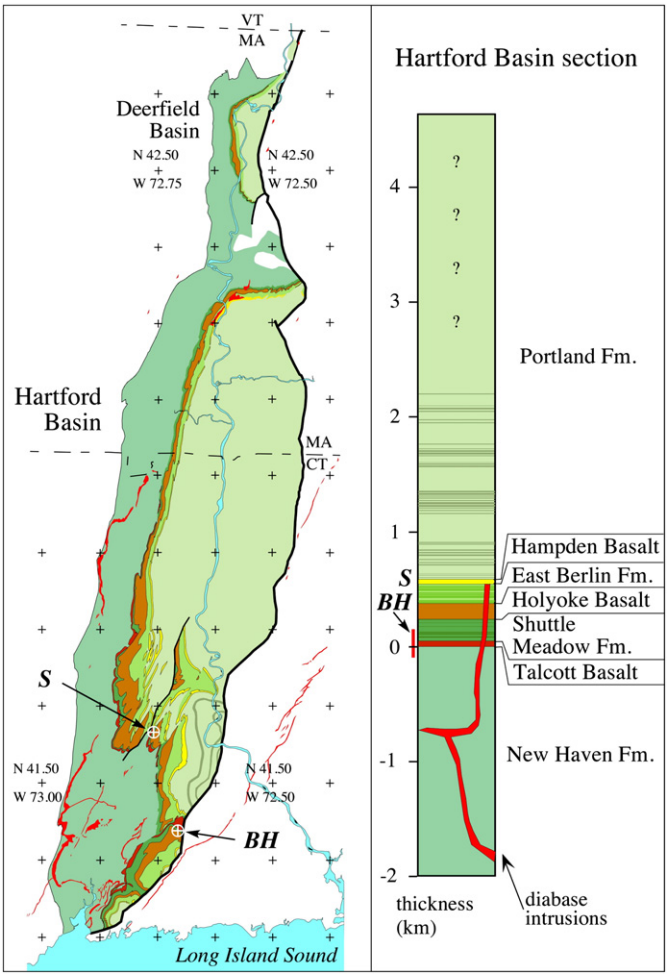

Fig. 3. Hartford basin geologic map and stratigraphic section showing position of Shuttle Meadow Formation, Bluff Head Bed (BH) and Silver Ridge Cores (S, and red line next to stratigraphic column). Modified from Kent and Olsen (2008).

correlative with the Orange Mountain Basalt of the Newark basin and the North Mountain Basalt of the Fundy basin. The North Mountain and Orange Mountain basalts are exactly correlative based on detailed palynology of the underlying strata (Fowell and Olsen, 1993; Fowell and Traverse, 1995; Olsen et al., 2003a), magnetostratigraphy (Kent and Olsen, 2000; Kent et al., 1995), and igneous petrology (Puffer, 1992). The Talcott Formation is geochemically indistinguishable from the Orange Mountain Basalt (Puffer et al., 1981), and the cyclostratigraphy of the Shuttle Meadow Formation and overlying units is nearly identical to that of the Orange Mountain Basalt and overlying units in the Newark basin (Olsen et al., 1996a, 2003a; Whiteside et al., 2007). Therefore, the age of the Talcott Formation must be very closely comparable to the age of the North Mountain basalt, which has produced an ID-TIMS U–Pb age of 201.3 ± .3 Ma (Schoene et al., 2006). Because the grains in this analysis were only air abraded and not chemically abraded, the reported age could be affected by Pb loss (e.g., Mattinson, 2005; Mundil et al., 2004), and the true age might be slightly older. The Holyoke Basalt, overlying the Shuttle Meadow Formation is geochemically identical to the lower Preakness Basalt of Newark basin (Puffer et al., 1981) and in an identical cyclostratigraphic position (Whiteside et al., 2007). The cyclostratigraphy of both the Shuttle Meadow Formation and the Feltville Formation indicates the same duration of about 270 ky, and the Preakness Basalt has produced a high-precision U–Pb age in agreement with this correlation (Blackburn et al., 2009). Thus, the numerical age of the lower Shuttle Meadow Formation is constrained to between 201.3 and 201.0 Ma.

The nominal relative age of the Shuttle Meadow Formation is less well constrained. Since the 1970s, the Shuttle Meadow Formation and all of the overlying CAMP flows (Talcott and Holyoke basalts) and sedimentary strata have been regarded as Early Jurassic in age, based on palynological correlation, vertebrate biostratigraphy, and radioisotopic ages (Cornet and Traverse, 1975; Olsen and Galton, 1977). However, the recent designation of the base-Hettangian (and hence base-Jurassic) GSSP has by definition made any determination of nominal age very difficult. The Triassic/Jurassic Boundary Working Group of the International Subcommission on Jurassic Stratigraphy of the International Commission on Stratigraphy (Morton, 2008a,b; Morton et al., 2008) voted to accept the proposal of Hillebrandt et al. (2007) to place the GSSP of the base of the Hettangian (and therefore the Triassic–Jurassic boundary) at the first occurrence of the ammonite *Psiloceras* cf. *spelae* in the Kuhjoch section in Austria. This first occurrence point defines the base of the Jurassic well above the main extinction interval, previously informally considered the boundary marker. Thus, the extinction is now wholly within strata of latest Triassic age, not at the boundary, and should be referred to as

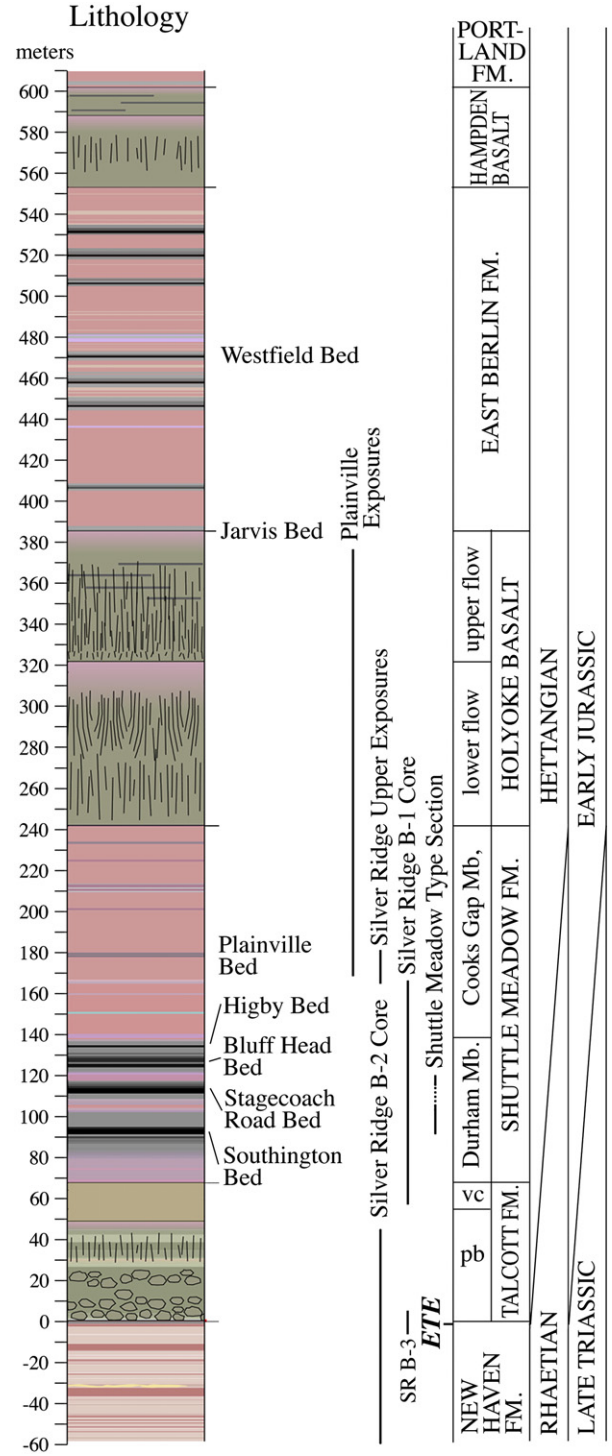

Fig. 4. Stratigraphy of Hartford basin Extrusive zone showing stratigraphic position of cores and outcrops (thickness normalized to lower Portland Formation: adapted from Whiteside et al., 2007 and Kent and Olsen, 2008). Abbreviations are: ETE, end-Triassic extinction event; pb, pillow basalt member of the Talcott Formation; SR B-3; vc, volcanoclastic member of the Talcott Formation.

the "end-Triassic extinction event" (ETE), as used here. This has the unfortunate and unintended consequence of making secure correlation of the newly defined Triassic–Jurassic boundary to continental environments exceedingly difficult. Although the extinction level is marked by a number of useful associated phenomena allowing global correlation in both marine and continental environments, such an the initial isotopic excursion (Hesselbo et al., 2002), a flood of the pollen taxon *Classopollis meyeriana* (Bonis et al., 2010), and an adjacent underlying thin zone of reverse magnetic polarity (Kent et al., 1995), the first occurrence datum of the ammonite *Psiloceras* cf. *spelae* occurs with no distinctive additional correlative records or events, and *P. spelae* itself is known from only a few marine sections globally.

What can be securely inferred at this time is that the lower Shuttle Meadow Formation is very close in age to the Triassic–Jurassic boundary, probably just older than it, deposited during the latest Rhaetian, beginning less than 50 ky after the ETE. This placement is based on correlation using stable carbon isotopes described by Whiteside et al. (2010), and available radioisotopic ages of CAMP units correlative to the Talcott Formation (Schoene et al., 2010) that can be directly compared with the numerical age of the base of the extinction level in marine strata (Schaltegger et al., 2008). Thus, the current status of the age of the Shuttle Meadow Formation conforms rather closely to the age inferred by Cornet et al.'s (1973) initial detailed study.

3. Materials and methods

This paper is largely based on two sets of materials: fossils and sediment samples collected at excavations of outcrops at Bluff Head (Figs. 1 and 4) from the Bluff Head Bed; and the Silver Ridge B-1, B-2, and B-3 cores, that together span most of the New Haven, Talcott, and lower Shuttle Meadow formations.

3.1. Bluff Head excavations

The fossil fish locality at Bluff Head in the bed of the same name was first described by Davis and Loper (1891). Loper made a significant collection of fish and plants from this locality and deposited them in the collections at Wesleyan University and in the U. S. National Museum (McDonald, 1975). McDonald and Cornet relocated the locality in 1969. The locality consists of outcrops in and along a small north-flowing tributary to Hemlock Brook on the north face of Bluff Head, North Guilford, Connecticut. Exact locality information is available to qualified researchers from the authors. The land is currently owned by the Nature Conservancy in Connecticut and is termed the Bluff Head Preserve.

Excavations for fish and other fossils were carried out at the locality by Cornet and McDonald in 1970–1971 (Cornet et al., 1973; McDonald, 1975; Schaeffer and McDonald, 1978), by Olsen and McDonald in 1984, and by Huber and McDonald in 1994 (Fig. 5). Cornet and McDonald and Huber and McDonald collected ~4 cm diameter by ~100 cm long columnar sections spanning the entire Bluff Head Bed (Fig. 6) that were analyzed in this study. Cornet (2001) also compiled quantitative data on the vertical distribution of fish taxa through the approximately 5 m^2 excavation (Fig. 5). Because Cornet and McDonald were working on more weathered portions of the outcrop, Cornet was forced to use a plastic consolidant to stabilize some parts of his rock column, rendering it unsuitable for carbon isotopic analysis. The much less weathered rock column collected by Huber and McDonald was well-stored and in pristine condition, although there are several short gaps that were bridged using Cornet's samples. Cornet, Huber, and McDonald donated these columns to Lamont-Doherty Earth Observatory where they now reside. Most of the fish collection now resides in the Paleontological Research Institution (Ithaca, New York), although some are retained at the American Museum of Natural History (New York, New York), and in McDonald's personal collection (Westminster School, Simsbury, Massachusetts).

3.2. Silver Ridge cores

A series of three HQ (6.35 cm) diameter geotechnical cores were taken in 2002 at a site near the southern boundary of Berlin, Connecticut. The cores were drilled with a standard truck-mounted drilling rig with water used as lubricant, and donated to Lamont-

Fig. 5. Bluff Head excavation in 1973 with N.G. McDonald (right) and R.V. Demicco, Binghamton University (left). Darker layers near feet constitute the Bluff Head Bed.

Doherty Earth Observatory where they currently reside. Silver Ridge B-1 was spudded at 41.5850°N latitude, 072.7565°W longitude and spans the entire uppermost Talcott and lower Shuttle Meadow formations with a total depth of 113 m (371 ft—here and elsewhere original measurement dimensions are cited to retain original precision) (Fig. 7). Silver Ridge B-2 was taken at 41.5842°N latitude, 072.7608°W longitude and covers part of the upper New Haven and most of the Talcott formations with a total depth of 61 m (200 ft) (Fig. 7). Silver Ridge B-3 was taken at 41.5838°N latitude, 072.7609°W longitude and recovered the uppermost Talcott and lowermost Shuttle Meadow formations with a total depth of 60 m (196 ft) (Fig. 8). These cores provide the first complete view of the stratigraphy of the lower Shuttle Meadow Formation, which previously was not understood.

The Silver Ridge B-1 core was drilled during excavations for the Silver Ridge development and recovered a number of important fossils and structures that could be registered directly to the core stratigraphy. Representative sedimentary structures and fossils from the core and surrounding exposures are shown in Fig. 9.

3.3. Sampling

Roughly 5 mm wide, rectangular channel samples were collected through all available material from the Huber and McDonald column of the Bluff Head Bed using a Dremel tool diamond saw, assuring that the isotopic character was continuously sampled. The average stratigraphic thickness spanned by each section was 2 cm, with no sample spanning a thickness of more than 4.7 cm.

Samples were taken from the Silver Ridge B-1 core at 1.1 m (3.5 ft) intervals by cutting 1×2.5 cm plugs with a water-cooled diamond coring bit in a drill press. The sample spacing was designed to allow each lithologic cycle (believed to be forced by climatic precession [~20 ky]) to be sampled at a rate of about 1 sample/ky, thus assuring that the Milankovitch cyclicity was not aliased. Depth data were recorded and analyzed in decimal feet, the US industry standard units marked on the core at the time of drilling and retained here to avoid loss of precision and ease of registry to the cores.

3.4. Analytical methods for bulk carbon isotopes

The bulk organic matter of samples from the Silver Ridge cores and the Bluff Head outcrop was analyzed by mass spectrometry to determine the ratio of $^{13}C/^{12}C$. Samples were cleaned with deionized water, air-dried, ground into a fine powder with a ceramic mortar and pestle, fumed with 37% HCl in a bell jar at 60 °C for 50 h, and dried above a plate of silica gel desiccant at 60 °C for at least 24 h. Although others have reported carbon loss due to heating, this did not occur in step-wise heating experiments conducted for this work, and extended heating was the only method that quantitatively removed recalcitrant dolomite from the samples. All samples were weighed into silver capsules, with mass determined by total organic-carbon (TOC) content, grouped according to TOC, and processed with an automated micro Dumas combustion technique using a Europa ANCA system plumbed into a 20–20–NT continuous flow mass spectrometer system at Lamont-Doherty Earth Observatory (Sambrotto lab). C isotope ratios were measured against NIST and IAEA standard reference materials that were combusted in the same manner as the samples (glucosamine, $\delta^{13}C=-20.80$, $C=20.50\%$; methionine, $\delta^{13}C=-25.10$, $C=40.25\%$, all versus the PeeDee Belemnite (PDB: $^{13}C/^{12}C=11237.2\pm60\times10^{-6}$), and are expressed in the standard "del" notation where $\delta^{13}C=[[(^{13}C/^{12}C)\ \text{sample}/(^{13}C/^{12}C)\ \text{PDB}]-1]\times1000$. Precision of the analytical system is 0.12‰ for C at the typical sample sizes (4 μm C) used here. Results are given in Appendix A.

3.5. Analytical methods for compound-specific carbon isotopes (*n*-alkanes)

N-alkanes were ultrasonically extracted from ~20 to 150 g of powdered sedimentary rock samples using a solvent system of decreasing polarity (methanol–dichloromethane, 1:1 v/v; hexane–dichloromethane, 4:1 v/v). Supernatants were recovered after centrifugation and pooled to yield a total lipid extract. The solvents were removed by rotary evaporation, and the extract was separated into three fractions on SPE cartridges (1 g silica-gel, 5% deactivated, 100–200 mesh topped with ~2 g anhydrous Na_2SO_4 to remove traces of water) with hexane (hydrocarbon fraction), hexane–dichloromethane (4:1 v/v), and DCM (polar fractions) as eluents.

The hydrocarbon fraction was further fractionated into adduct (straight chain ($C\geq14$) *n*-alkanes) and non-adduct fractions by urea adduction. The adducted fraction was quantified using gas chromatography (GC) and the compound identification confirmed by GC-mass spectrometry (GC-MS). GC analysis of *n*-alkanes was performed on a HP 5890 II GC fitted with a flame ionization detector. GC-MS analysis was carried out on a Thermo Finnigan GC-ToF-MS. The recovered fractions contained almost exclusively a mixture of *n*-alkanes. Compound-specific carbon isotopic measurements were determined by isotope ratio monitoring-gas chromatography/mass spectrometry (irm-GC/MS) using a Finnigan MAT DeltaPlus MS coupled to a Hewlett Packard 6890 GC via a combustion interface. The $\delta^{13}C$ values for individual compounds were calibrated based on co-injection of internal reference standards and introduction of reference CO_2 gas pulse, reported as means of duplicate runs ($\sigma=\pm0.3$ to 0.6), and expressed in ‰ relative to PDB in del notation as above. Results of the *n*-alkane analyses are tabulated in Appendix A.

3.6. Time series analysis

Time series of lithology (rock color), interpretative relative water depth (depth ranks), and geochemical (TOC, $\delta^{13}C_{org}$) properties of the Silver Ridge B-1 core were analyzed using Analyseries v2.0.4 for Macintosh (Paillard et al., 1996). Color data were collected subjectively in four categories arranged as a series of red (0), purple (1), gray (2), and black (3) continuous intervals. These colors correspond roughly to moderate reddish brown 10R 4/6, pale red purple 5RP 6/2, medium gray N5, and black N1 of the Munsell color chart (Munsell Color, 2009). Depth ranks are a classification of suites of sedimentary structures and fabrics (facies) assigned ranks along a scale of interpreted increasing relative water depth. Here the depth ranking scheme of Olsen and Kent (1996) is used, where values range from 0 (a massive mudcracked mudstone: the shallowest water facies) to 5 (microlaminated calcareous mudstone to limestone: the deepest water facies). As for colors, depth rank data were collected in continuous intervals. The chemical data, color

data, and depth rank data were interpolated to 0.003 m (0.01 ft), detrended, and transformed using the periodiogram (FFT-square window) option of Analyseries. The Analyseries filtering option was used to Gaussian filter the data at frequencies of 0.0650787 and 0.1201476 cycles/m (0.019836 and 0.036621 cycles/ft), and a bandwidth of 0.019685 cycles/m (0.006000 cycles/ft) corresponding to the main peaks revealed by the spectral analysis.

4. Results

4.1. Bluff Head Bed

The excavations of S. W. Loper, B. Cornet, N. G. McDonald, P. Huber and others at the Bluff Head locality produced thousands of remarkably preserved holostean, palaeonisciform, and coelacanth fishes as well as other fossils (Davis and Loper, 1891; McCune et al., 1984; McDonald, 1975; Olsen and McCune, 1991; Olsen et al., 1982) including the large coelacanth *Diplurus longicaudatus*, the holostean *Semionotus*, the paleonisciform *Ptycholepis*, and the redfieldiid paleonisciform *Redfieldius* (Fig. 10). The data from these excavations show distinct vertical trends in assemblage composition of higher-level taxa that correlate with changes in lithology and $\delta^{13}C_{org}$ (Fig. 11).

The lithology of the Bluff Head Bed at Bluff Head is dominated by microlaminated, organic-rich (TOC = ~4.4%) micritic mudstones interbedded with thin, normally graded, blocky-weathering layers of siltstone and silty sandstone of arkosic composition, interpreted as turbidites (Fig. 9) which are often abundant in lakes (e.g. Forel, 1885; Johnson, 1984; Pettijohn et al., 1972). Assuming the light–dark couplets with microlaminated units are varves deposited below the chemocline in a chemically stratified lake, the bed at the Bluff Head site represents ~3000–4000 yr of continuous sedimentation (Dickneider et al., 2003). The assumption that these couplets are varves are based on comparisons to very similar couplets in modern chemically stratified water bodies for which there is a vast literature (e.g. Anderson and Dean, 1988; Bogen and Wilson, 1994; Cooper et al., 2000; Dean, 2006; Dean et al., 1999).

The lowest 11 cm of the Bluff Head Bed is well laminated but produced no fish in the collected quantitative data from the Cornet excavation. However, a small number of well-preserved *Semionotus* were found in subsequent excavations. Dominant taxa in the lowest strata for which there are available quantitative data include *Redfieldius* with fewer *Semionotus* (Fig. 11). The immediate overlying units are well-microlaminated with the highest carbonate content (up to 64% by mass) in the section and are strongly dominated by *Redfieldius*, whereas *Semionotus* is absent. The upper units are less well microlaminated, have a lower carbonate content, are dominated by *Semionotus*, and completely lack *Redfieldius*. The last appearance of the latter taxon occurs at the base of a major turbidite (Fig. 11), at about 50 cm above the base of the bed. As a generalization, *Redfieldius* is dominant in the more microlaminated intervals with higher carbonate content, whereas *Semionotus* is dominant in the more clay rich, less well-laminated beds as clearly shown in Fig. 12.

The abundance of large (2–10 cm) phosphatic coprolites correlates directly with the abundance of *Redfieldius*. These coprolites were probably produced by the large (~1 m) coelacanth *Diplurus longicaudatus* present in the same units because morphologically identical coprolites have been found within *Diplurus* from the Deerfield basin (Gilfillian and Olsen, 2000), and may indicate that *Redfieldius* was its preferred prey. *Ptycholepis* occurs sporadically through the section but is most abundant

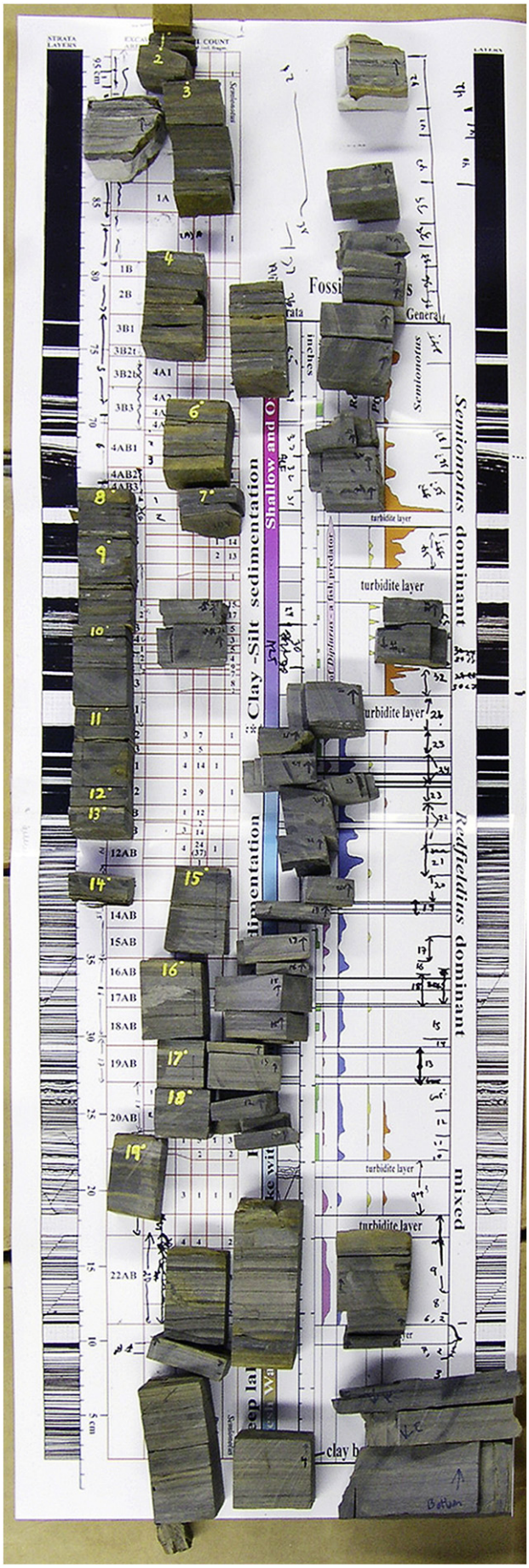

Fig. 6. Bluff Head column samples on top of full-scale diagram of the section by Cornet (2001). Column samples of B. Cornet have yellow numbers; Column samples of P. Huber have black numbers. There were some places where there was duplication within a column, because of small-scale penecontemporaneous faulting and these have been accounted for. The horizontal alignment of the samples is consequence of duplicate samples.

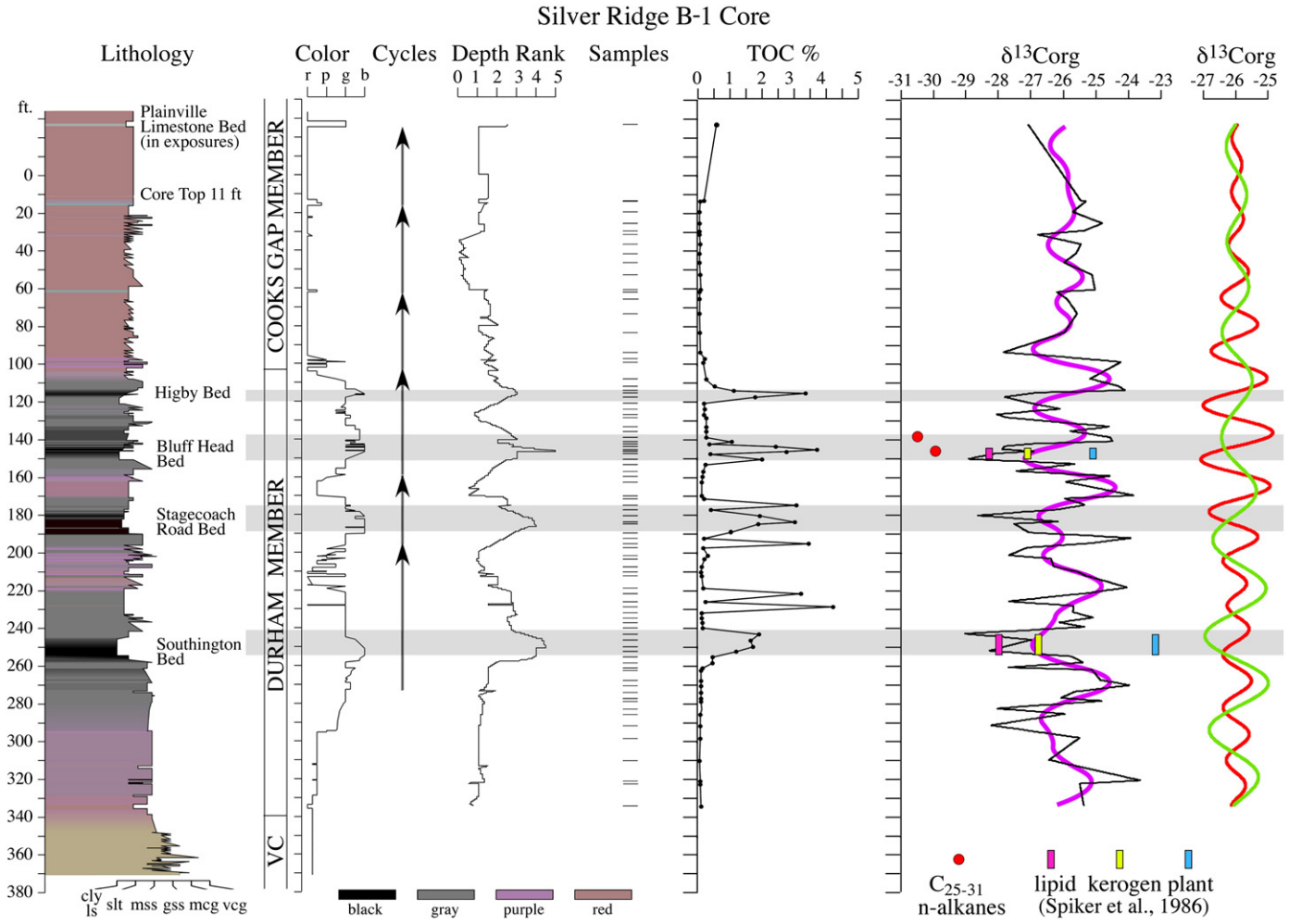

Fig. 7. Silver Ridge B-1 core. Abbreviations are: b, black; cly ls, claystone or limestone; g, gray; gss, gravelly coarse sandstone; mcg, medium conglomerate; mss, medium sandstone; p, purple; r, red; slt, siltstone; VC, volcanoclastic member of the Talcott Formation; vcg, very coarse conglomerate.

in association with *Semionotus*. It is only common over a 1‰ range of $\delta^{13}C_{org}$ values (−27.5‰ to 27.6‰).

Overall, the $\delta^{13}C_{org}$ record tracks the changes in fish assemblage composition (Fig. 11). The most prominent changes (over a few centimeters) occur at about the 10 and 50 cm level, synchronous with the first and last occurrences of *Redfieldius*, respectively. In summary, the zone with high carbonate content and a high degree of microlamination is associated with *Redfieldius* and relatively positive $\delta^{13}C_{org}$ values, whereas relatively negative $\delta^{13}C_{org}$ values characterize the zones dominated by *Semionotus*.

Three (3) samples from the Bluff Head Bed at Bluff Head were analyzed for *n*-alkane carbon isotopic composition (Appendix A). The average $\delta^{13}C_{alk}$ for the weighted mean odd C_{25}–C_{31} *n*-alkanes of these three samples is −29.61‰, which differs by 0.32‰ from the approximately stratigraphically equivalent deep-water unit sampled in the Silver Ridge core.

4.2. Cyclicity

Lacustrine strata within the eastern North American rift basins are comprised of distinct sedimentary cycles that reflect the rise and fall of very large lakes paced by Milankovitch climate changes (Hubert et al., 1976; Olsen, 1986; Olsen and Kent, 1999; Van Houten, 1964; Whiteside et al., 2007). Attributed to changes in precipitation controlled by the climatic precession cycle that theoretically averaged ~20 ky at the end of the Triassic (Berger et al., 1989; Olsen and Whiteside, 2008) (Fig. 7), the fundamental sedimentary sequence is termed a Van Houten cycle, after its discoverer (Olsen, 1986). The Bluff Head Bed is the deepest-water phase of one of these cycles (Fig. 4).

The expression of these lithological cycles tracks lower frequency oscillations that are ascribed to lower frequency precession-related cycles. The most prominent of these are the short modulating cycle (~100 ky), the McLaughlin cycle (405 ky), and the long modulating cycle (1.75 my; Olsen and Kent, 1996, 1999). Within the Shuttle Meadow Formation, as is true for other post-ETE units, the McLaughlin cycle is vertically thicker than the formation itself, in this case overlapping into the underlying New Haven Formation. The stratigraphy of the Silver Ridge B-1 core has already been typologically described in terms of these cycles (e.g., Olsen et al., 2003b) (Fig. 7), and time series analysis corroborates this descriptive approach.

Fourier analysis of the color, depth rank, and TOC data revealed similar and coherent periodicities (Fig. 13) at ~17 m (~56 ft), the same thickness that were typologically picked for the Van Houten cycle (Fig. 7), and at ~112 m (~368 ft), which although not formally statistically significant, is close to predicted for the short modulating cycle. However, there is also a strong periodicity at about 11 m (36.4 ft), which is nearly half of a single Van Houten cycle. This periodicity is reflected in the presence of the Higby Bed, a weakly developed fish-bearing laminite midway through the same Van Houten cycle that also contains the Bluff Head Bed.

The $\delta^{13}C_{org}$ stratigraphy of the Silver Ridge cores show strong cyclicities with large fluctuations (0.03% to 4.9% and −24‰ to −29‰) and an overall pattern much more complex than the depth rank data

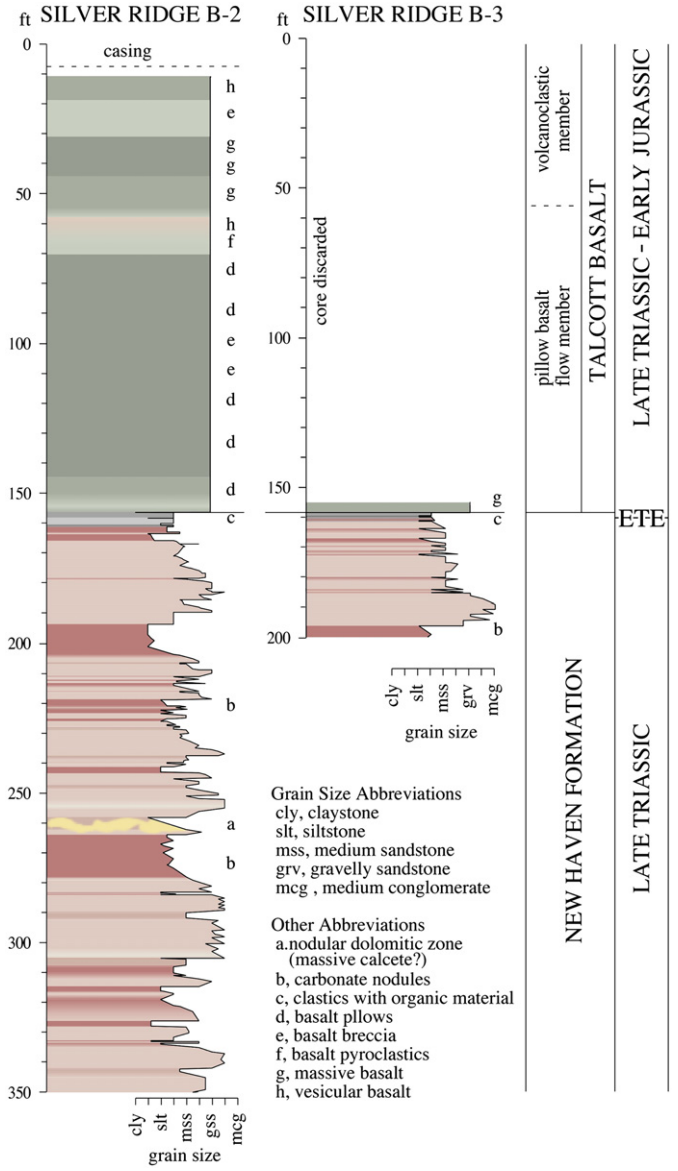

Fig. 8. Silver Ridge cores B-2 and B-3. Abbreviations for grains size: cly, claystone; slt, siltstone; mss, medium sandstone; gss, gravelly coarse sandstone; mcg, medium conglomerate. Lithological colors as in Fig. 7, except for yellow which represents a yellowish nodular carbonate.

(Fig. 7). More negative $\delta^{13}C_{org}$ values (~−29‰) occur in the dark gray and black units with high depth ranks and high TOC (>2%), which are interpreted as deeper water. The red beds and light gray beds deposited in shallower water tend to have more positive (^{13}C enriched) $\delta^{13}C_{org}$ values (~−25‰) and much lower TOC (<0.5%), with some exceptions in sandy or silty units [e.g. 67.51 and 69.65 m (221.5 and 228.5 ft)] containing macroscopic vascular plant remains (phytoclasts). Phytoclasts and microscopic woody particles are abundant in the Shuttle Meadow Formation, which is a reflection of the importance of allochthonous organic carbon in the Shuttle Meadow lacustrine deposits. Overall, the magnitude of the fluctuations in both TOC and $\delta^{13}C_{org}$ are larger in the gray and black strata than in the red beds, and more than twice as many stratigraphic cycles were identified in the geochemical data than defined by the lithologically and typologically defined Van Houten cycles (Fig. 7).

Comparison of the power spectra of depth rank, TOC, and $\delta^{13}C_{org}$ displays both striking similarities and major differences (Fig. 13). The strong spectral peaks with periods of 9.8 m (32.3 ft) and 8.4 m (27.4 ft)

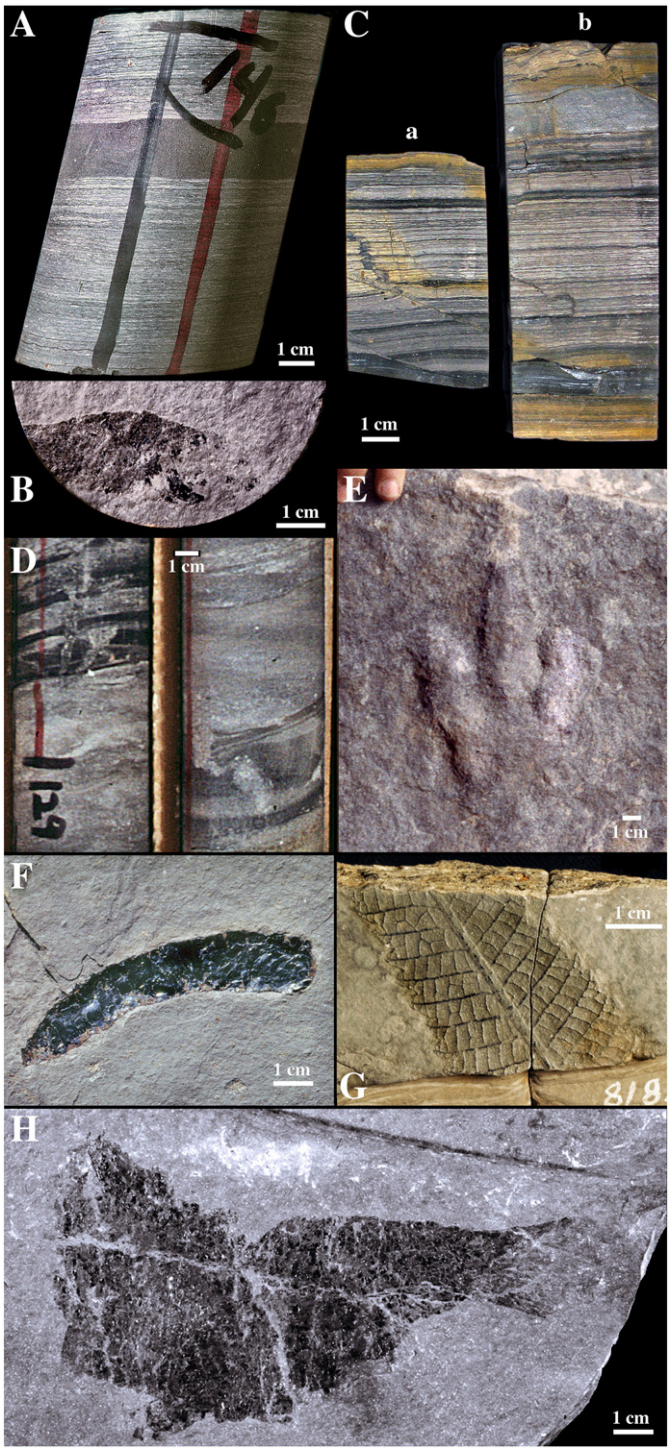

Fig. 9. Representative sedimentary structures and fossils from the Silver Ridge B-1 core and surrounding exposures. A, Segment of the Silver Ridge B-1 core (146 ft) showing the typical carbonate-rich microlaminated Bluff Head bed with turbidite at 146.1 ft. B, Lower bedding plane surface of core segment shown in A with a anterior portion of a poorly preserved by completely articulated Semionotus. C, Comparison of portions of the Bluff Head excavations in the Bluff Head Bed shown ease of correlation of microlaminate from column to column with segments collected about 3 m apart: a, B. Cornet column segment unit 22AB spanning 11–17 cm in Fig. 11; b, P. Huber column segment spanning 8–20 cm in Fig. 11 (note turbidite in upper part). D, Examples of portions of Silver Ridge B-1 core (129 and 130.5 ft) showing desiccation cracks. E, Natural cast in fine sandstone of theropod dinosaur footprint (c.f., Eubrontes (Anchisauripus) tuberatus) from just below Southington Bed, Silver Ridge outcrops. F, Coprolite of Diplurus longicaudatus from Bluff Head excavation of Bluff Head Bed. G, Portion of frond of fern Clathropteris meniscoides from Bluff Head Bed at Durham fish locality (41.4282°N, 72.7260°W) (Wesleyan University Geology collection no. 818) collected by S. Ward Loper). H, Complete articulated Semionotus from the Southington Bed, Silver Ridge outcrops.

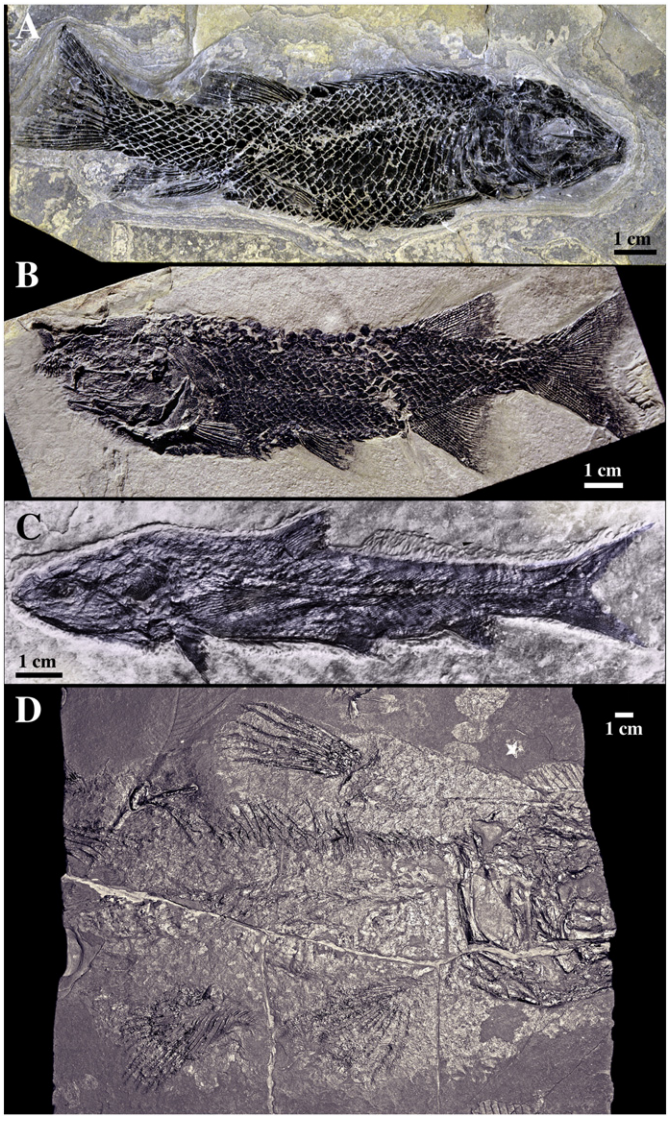

Fig. 10. Representative fish taxa from the Bluff Head Bed: A, *Semionotus* sp. (N.G. McDonald collection); B, *Redfieldius* sp. (N.G. McDonald collection); C, *Ptycholepis marshi* (Wesleyan University Geology 907): from Schaeffer et al., 1975); D, *Diplurus longicaudatus* (AMNH 627: from Schaeffer, 1948).

in the $\delta^{13}C_{org}$ data coupled with relatively little power in the lower frequencies contrast with indistinguishable frequencies in the depth rank and TOC spectra (although magnitude of the power in the % TOC data, like the $\delta^{13}C_{org}$ data are not as red-shifted as the depth ranks). This contrasts with the color and TOC spectra, where most of the power is concentrated in the lower frequencies, although there are smaller spectral peaks similar to these seen in the $\delta^{13}C_{org}$ data and vice versa. The major difference in the partitioning of power between lower and higher frequencies is explicable by the strongly symmetrical $\delta^{13}C_{org}$ data, in which low frequency fluctuations appear as a modulation of the amplitude of the higher frequencies. In these data, the lower frequency cycles are more or less invisible to Fourier analysis. On the other hand, the depth rank and color data are strongly asymmetrical, hence, the variance is in the lower frequencies (Fig. 13). These lower frequencies have periods nearly as long as the length of the data and are consequently not formally significant (although they are probably real patterns rather than noise).

Cross-spectral analysis shows the greatest coherency (variations which have similar spectral properties) at frequencies corresponding to 13.6 and 16.1 m (Fig. 13). Filtering the depth rank and $\delta^{13}C_{org}$ data at these two frequencies shows that they explain most of the variability in the data when the two filtered series are summed and compared at the same scale (Fig. 7). Both the raw and filtered data show that in the intervals with highly variable depth rank and $\delta^{13}C_{org}$, the most ^{13}C depleted portions of the curve correspond to the deepest water, main fish-bearing units (Fig. 7), notably the Southington Bed, Stagecoach Road Bed, Bluff Head Bed, and Higby Bed.

In addition to $\delta^{13}C_{org}$, *n*-alkanes from 2 samples from the Silver Ridge B-1 core were analyzed (Figs. 7 and 14; Appendix A) to test the hypothesis that the $\delta^{13}C_{org}$ data were not representative of atmospheric values (see below). One sample was from the very dark gray microlaminated deep-water Bluff Head Bed at 44.58 m (146.25 ft) and the other was from a medium gray thin-bedded siltstone with desiccation cracks from the shallow-water phase of the same cycle at 42.29 m (138.75 ft). The results for the homologous *n*-alkanes from each sample were within 0.6‰ of each other, and the standard deviation for the all the C_{25}–C_{31} *n*-alkanes from the two samples was within 0.01‰ of each other. However, the flame ion detector traces (FID traces) of the two samples look very different (Fig. 14). Specifically, the proportion of *n*-alkanes of long chain length ($>C_{20}$) with a probable leaf wax origin in the shallow-water sample was much higher than that in than in the deep-water sample, consistent with a relative lack of organic material of phytoplankton origin in the shallow-water sample. The most abundant *n*-alkanes in the deep-water sample are the C_{15}–C_{17} *n*-alkanes, consistent with a major phytoplankton component. The differences between the abundances of the various *n*-alkanes indicate they are indigenous, given their physical proximity to each other. Although the $\delta^{13}C_{alk}$ values for the C_{25}–C_{31} *n*-alkanes from the shallow- and deep-water samples are very similar (<0.5‰), the $\delta^{13}C_{org}$ values of the same samples differ by nearly 3‰, with the shallow-water sample ($\delta^{13}C_{org} = -24.78$‰) more ^{13}C enriched than the deep-water sample ($\delta^{13}C_{org} = -27.07$‰).

5. Discussion

In this paper the discussion is focused on examining the results of analyses from the smallest scale, the Bluff Head Bed, to cyclicity of the Shuttle Meadow Formation, to the largest-scale, which involves the effects of the CAMP eruptions and concurrent extinctions. This order also tracks from the general and cyclical to unique historically contingent processes.

The most distinct feature of the $\delta^{13}C_{org}$ data and distribution of fish taxa is that the relatively more ^{13}C-enriched interval is dominated by *Redfieldius*. The fact that the microlaminations are best developed in this interval that is bounded on either side by *Semionotus*-dominated zones suggests that the *Redfieldius*-dominated interval is the deepest water part of the Bluff Head Bed. The simplest hypothesis for this pattern is that these data reflect an efficient biological pump operating during maximum lake depth and the time of most stable perennial water column chemical stratification (meromixis). Given the carbonate-rich nature of the *Redfieldius*-bearing unit compared to the *Semionotus*-rich intervals above and below, this interval was probably deposited in water of higher solute content as well.

Redfieldius has a long subterminal mouth, with eyes well in front of the jaw join as is primitive for the Paleonisciformes and actinopterygians in general (Kriwet, 2001; Lauder, 1980). This morphology suggests a ram-feeder with a planktivorous diet analogous to extant anchovies, and consistent with its presence as the most abundant fish in the deepest water unit (Fig. 15). Breakdown of meromixis would reduce the efficiency of the biological pump and cause frequent mixing of the epilimnion and hypolimnion, resulting in more ^{13}C depleted values, as observed in the data. *Semionotus* might be expected to become prevalent during times of oxygenation of the lake bottom, such as during times of lake transgression (0–35 cm, Fig. 11) and regression (50 to +100 cm, Fig. 11) because it has features typical of extant fish that are suction feeding generalists feeding at or near the bottom, or shore, or in mid water (Fig. 15), such

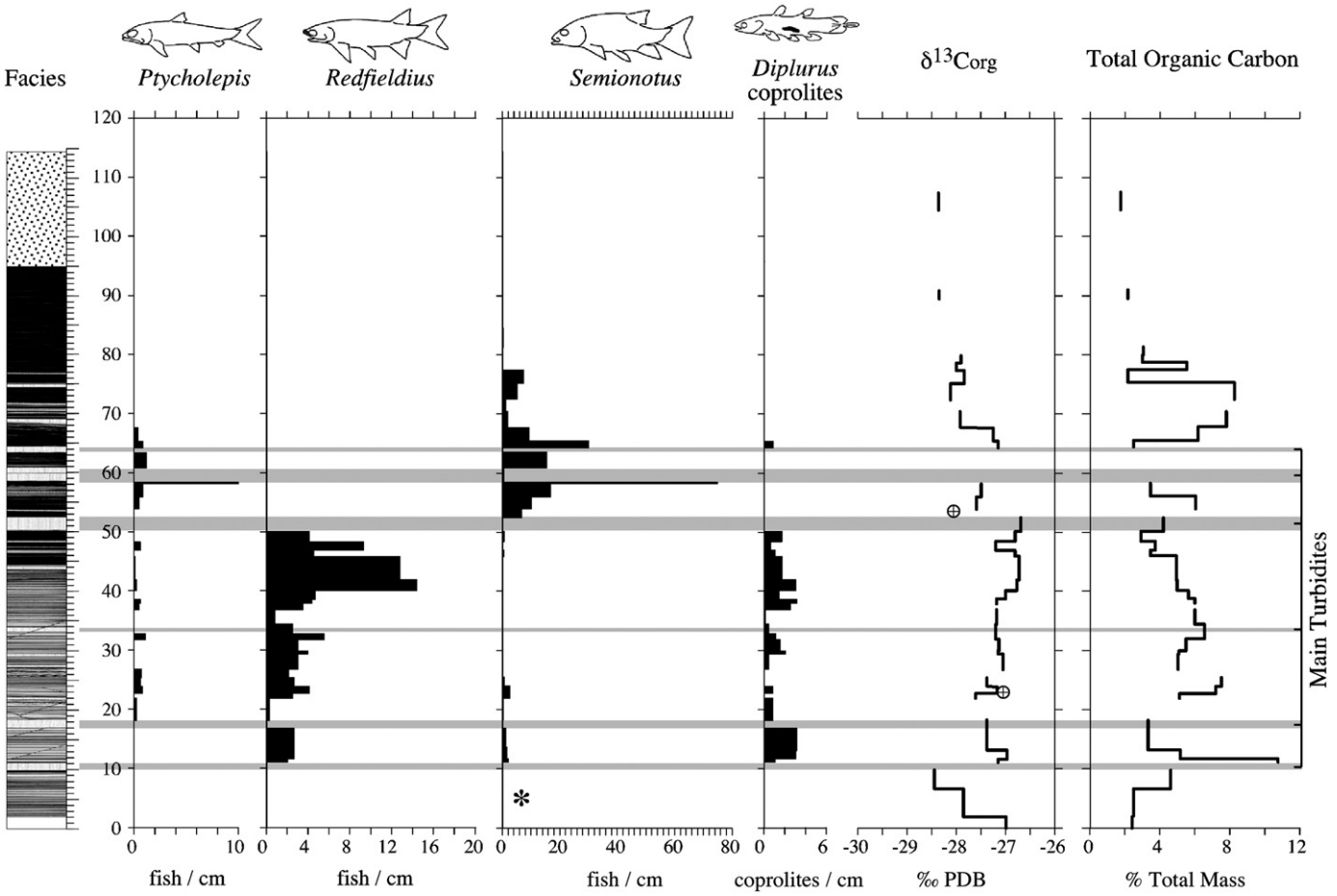

Fig. 11. The Bluff Head Bed excavation Distribution and abundances of fish and coprolites and $\delta^{13}C_{org}$ and Total organic carbon (TOC) data from the Bluff Head Bed excavations at Bluff Head. * indicated the presence of *Semionotus* without quantitative data. Circles with the crosshair indicate very approximate position of $\delta^{13}C_{org}$ values from the Silver Ridge B-1 core at 145.26 and 146.25 ft showing that mid-laminite $\delta^{13}C_{org}$ values at Silver Ridge are more ^{13}C enriched that values in less well-laminated strata still within the laminite. Correlation is based lining up the transition between microlaminated and non-microlaminated in the core and excavation and assuming equal accumulation rates, which are regarded as conservative. This is probably incorrect and the accumulation rate at Bluff Head is almost certainly more than at the Silver Ridge site, but if correlation of the upper sample from the Silver Ridge core is higher in the Bluff Head section than indicated here, it will only make the correspondence of the values closer.

as a relatively small mouth with a free maxilla, low on the head, and lack of specific adaptations for planktivory or piscivory. Semiontoids specifically have been interpreted as suction feeders (Lauder, 1982; Patterson, 1973).

In the Bluff Head Bed, the more ^{13}C enriched values of autochthonous organic carbon reflect higher degrees of lake stratification that might correlate with specific and repeatable changes in the fish community, such as the disappearance of *Redfieldius* and the dominance of *Semionotus*. This pattern has been reported in other sequences (Whiteside, 2006), including multiple Van Houten cycles within the Triassic Lockatong Formation of the Newark basin (Olsen, 1980), the Westfield Bed of the East Berlin Formation of the Hartford Basin (Fig. 4), and the Turners Falls fish bed of the Turners Falls Formation in the Deerfield basin (Gilfillian and Olsen, 2000). Similar patterns in lakes subject to climate forced fluctuations of any age should be expected. One possible example in a very similar context with similar facies are lacustrine cycles in the Devonian Orcadian basin of Scotland, one cycle of which also shows a trend to more positive values in the deepest water facies of the overall deep-water portions of the cycle (Stephenson et al., 2006).

Bulk $\delta^{13}C$ of organic matter in lacustrine sediments consists of an allochthonous component, principally dominated by various remains of terrestrial vascular plant material, and an autochthonous component comprised of autotrophic phytoplankton and aquatic heterotrophs. Aquatic angiosperms had not evolved in the early Mesozoic, so the contribution of aquatic macrophytes of the Shuttle Meadow lakes was presumably minor, although the sistergroup to plants, the charophytes, was sometimes common and made an unknown contribution to the organic matter. The woody component of terrestrial plants has $\delta^{13}C$ values that tend to be considerably more ^{13}C enriched than those for phytoplankton, depending on the taxonomic composition of the phytoplankton. Eubacterial heterotrophs and animals tend to reflect what they consume, but the Archaea, particularly methanogens, can be extremely depleted in ^{13}C (−60‰). The bulk $\delta^{13}C$ of the organic lacustrine sediments then is a mixture of these components and that mixture depends largely on relative inputs into the lake and the fate of those inputs due to the metabolism (i.e. ecosystem function) of the lake. Additionally, all of the inputs are expected to change their $\delta^{13}C$ values in response to changes in atmospheric $\delta^{13}C$, such as those that occurred during the strong carbon isotopic excursions associated with other mass extinctions (e.g., Holser and Magaritz, 1987; Hsü et al., 1982) as well as that at the end-Triassic (Hesselbo et al., 2002; Whiteside et al., 2010). These events include the ETE immediately preceding the deposition of the Shuttle Meadow Formation.

There are two other possible explanations that could account for the $\delta^{13}C_{org}$ trend observed through the Bluff Head Bed. The first is change in the taxonomic composition of the phytoplankton. Taxon-specific studies of $\delta^{13}C$ of lacustrine phytoplankton such as Vuorio et al. (2006) are uncommon, but show wide variation in isotopic

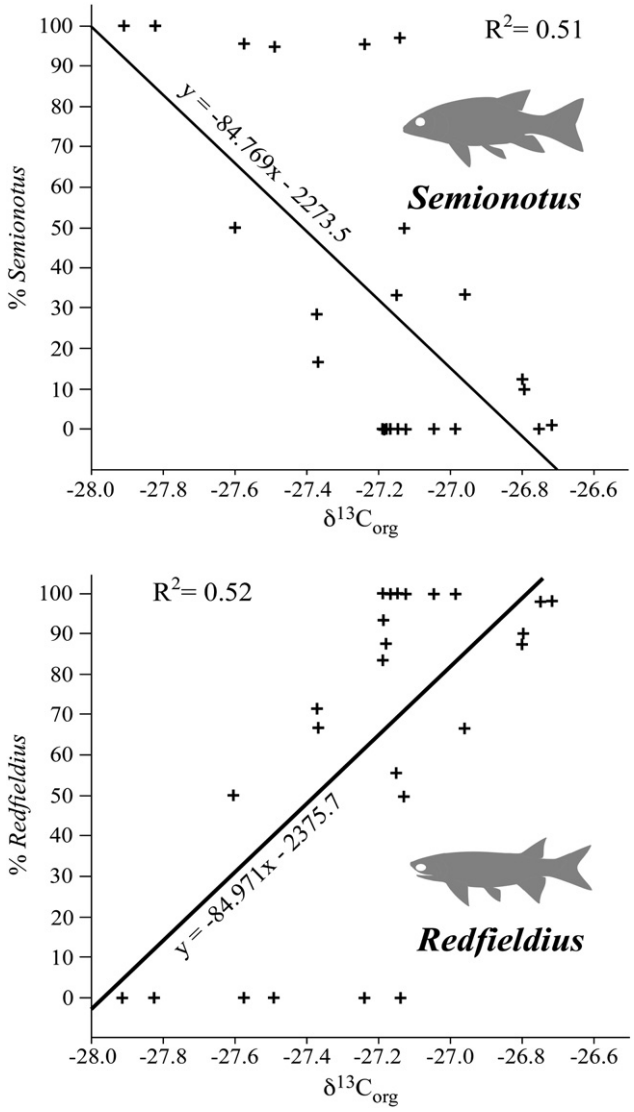

Fig. 12. Relationship between $\delta^{13}C_{org}$ of the Bluff Head bed and the percentage of *Semionotus* (above) and *Redfieldius* (below).

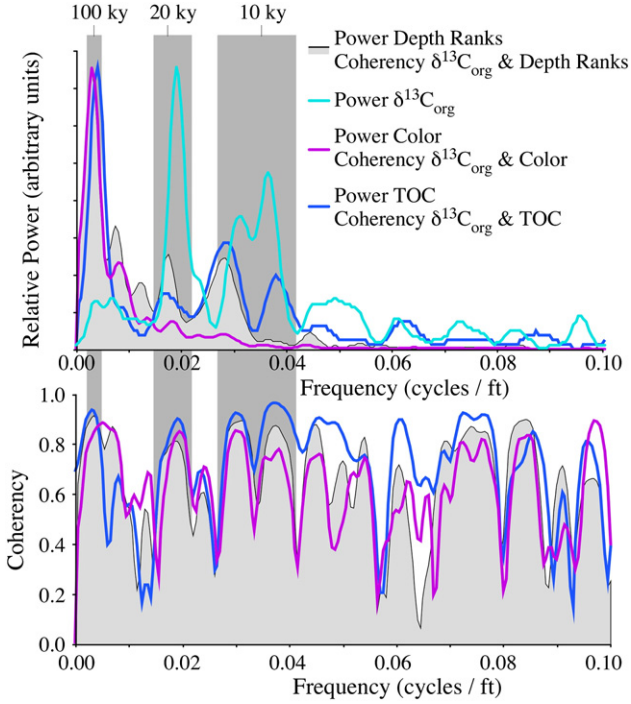

Fig. 13. Power spectra of the Silver Ridge B-1 core and cross-spectral analysis showing the coherency between various proxies. See text for explanation.

composition between different taxa of phytoplankton. Vuorio et al. (2006) demonstrated that green and golden algae (Chlorophtya and Chrysophyta *sensu stricto*) are the most ^{13}C depleted (~−32‰ to −34‰) whereas some cyanobacteria (*Gloeotrichia*) are very ^{13}C enriched (−8‰), with most cyanobacteria averaging about −26‰. Diatoms average about −30‰. There is no evidence, however, of early Mesozoic diatoms. The observed trends could be generated by a greater abundance of cyanobacteria during the deposition of the *Redfieldius*-bearing interval at high stand with stable stratification, with other autotrophs being relatively more abundant as the lake rose and fell with less stable stratification. However, this is the opposite of what would be predicted. Cyanobacteria are more likely to have been abundant during the lake fall as evaporation and the breakdown of stratification increased nutrient concentrations. This explanation is thus discounted, while still acknowledging that the composition of the phytoplankton that contributed organic matter to the Bluff Head Bed is essentially unknown. The second alternative explanation, which is more difficult to discount, is that the more carbonate rich waters that deposited the *Redfieldius* interval were depleted in CO_2 and the phytoplankton were using HCO_3^- as a carbon source (Espie et al., 1991). Again, this effect is largest in the cyanobacteria and they are most likely to have been more abundant during climatically forced lake fall.

Semionotus from the Bluff Head Bed exhibits an extremely large range of morphologies ascribed to in situ evolution of a species flock (McCune, 1981, McCune et al., 1984). Presumably, this explosive speciation indicates a high intrinsic rate of speciation, a taxon-specific characteristic. In this case, *Semionotus* speciated extremely quickly within the depauperate (at higher taxonomic levels) world of the ETE interval. However, this diversity is not uniformly distributed within the bed. Most of the morphological diversity occurs within the *Redfieldius* interval despite the fact *Semionotus* is much less common there, compared with the overlying *Semionotus*-dominated interval. *Semionotus* from the upper 30 cm of the bed shows little apparent variation (Cornet, 2001), presumably because of the extirpation of most of the species flock as the lake shrinks in size. This appears to be similar to the pattern described by McCune (1990) for the younger species flock from the Newark basin, correlative with the middle portion of the East Berlin Formation in the Hartford basin.

Although the deeper-water Bluff Head Bed shows a trend towards more ^{13}C enriched isotopic ratios in the deepest water phase, at the scale of multiple complete cycles, the lower Shuttle Meadow section does not seem to follow this model of lake stratification controlled by the efficiency of the biological pump. Instead, the $\delta^{13}C_{org}$ values are on the whole relatively ^{13}C-depleted in the deeper water intervals and enriched in the shallow water intervals (Fig. 7). The ~5‰ magnitude in $\delta^{13}C_{org}$ is hypothesized to be the result of the local mixing of carbon derived from different sources with different $\delta^{13}C$ values. As a result, the function of the biological pump would still be enhanced during high lake levels.

Originally, the $\delta^{13}C$ work was begun with the hope of detecting the carbon isotopic excursions associated with the end-Triassic extinction. A strong shift to depleted values in $\delta^{13}C_{org}$ was in fact discovered from a section in which the mass-extinction was recorded just below the oldest CAMP basalt (Whiteside et al., 2003, 2010). However, it was quickly discovered that the $\delta^{13}C_{org}$ fluctuations in the cyclical lacustrine deposits overlying the oldest CAMP basalt and above were larger in magnitude

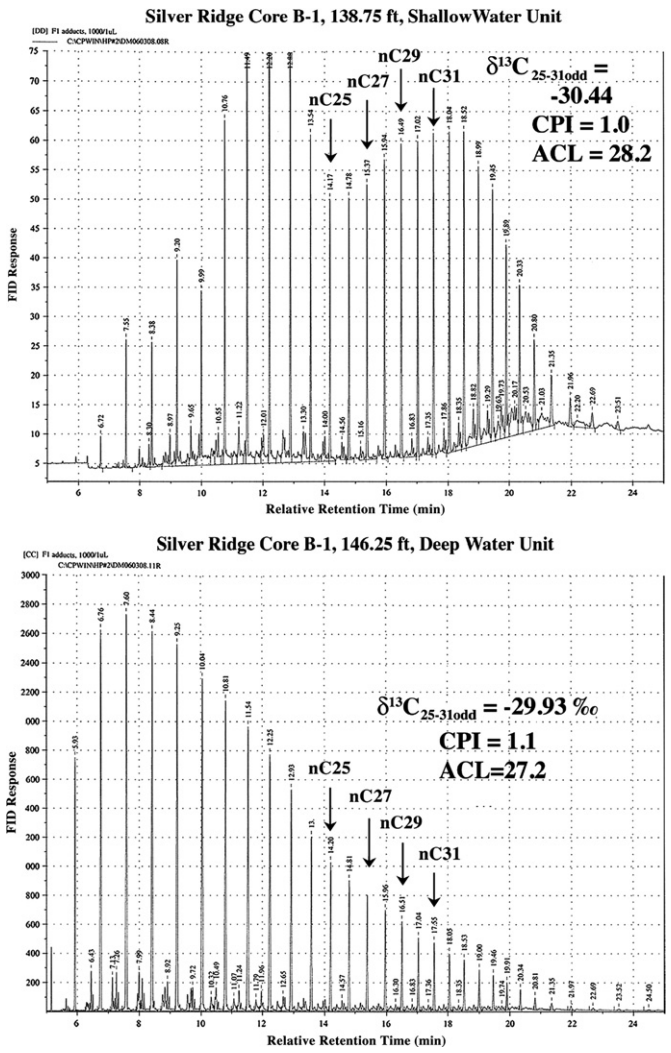

Fig. 14. Flame Ionization Detector (FID) trace of the saturate fraction of extractions of contrasting environments from the Silver Ridge B-1 core: A, deep-water microlaminated sample from the Bluff Head Bed with a $\delta^{13}C_{org}$ value of −27.07‰ produced by a meromictic lake—Silver Ridge Core B-1, 146.25 ft); B, shallow-water unit from the same Van Houten cycle exhibiting a $\delta^{13}C_{org}$ value −24.78‰—Silver Ridge Core B-1, 138.75 ft.

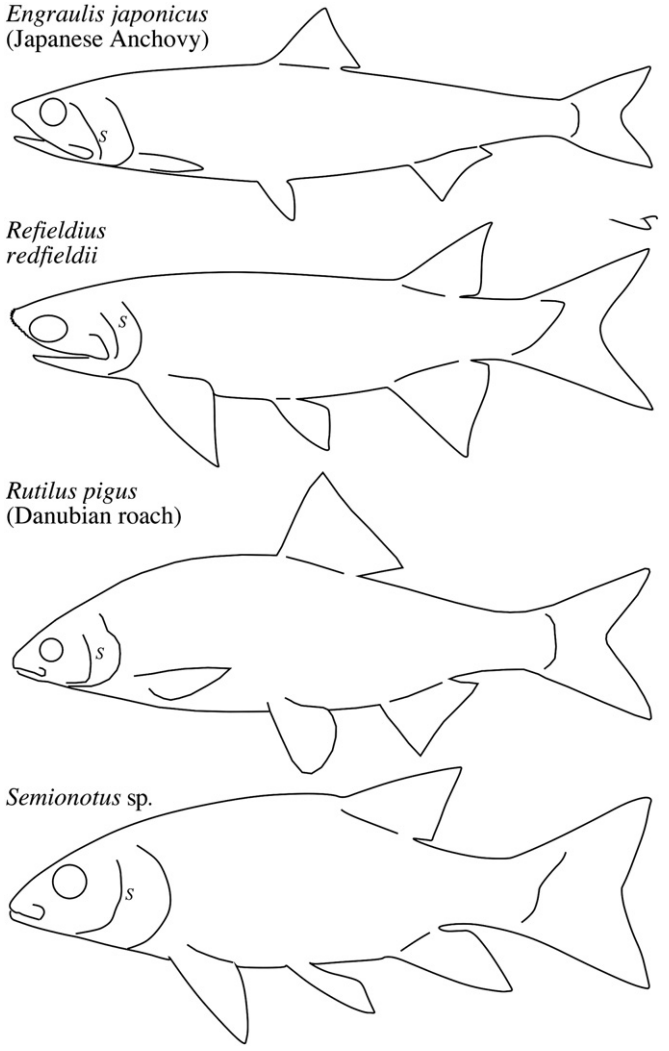

Fig. 15. Living taxa showing adaptations for planktonic ram feeding (*Engraulis japonicus*—Japanese Anchovy) and visually selective suction feeder (*Rutilus pigus*—Danubian roach) compared to fossil taxa discussed in text. The wide gape, small teeth, inclined suspensorium (S) seen in anchovies, and *Redfieldius* (and the other redfieldiids, are all associated with ram feeding (Lauder, 1980; Kriwet, 2001) planktivory. In contrast the small and subterminal mouth and the vertical suspensorium seen in *Rutilus* (many other cyprinids) and *Semionotus* (Lauder, 1982; Patterson, 1973), are associated with selective feeding at or near the bottom or on rocks. *Engraulis japonicus* is redrawn from Scandinavian Fishing Year Book ApS (2009); *Rutilus pigus* is redrawn from Seeley (1886); *Redfieldius* is redrawn from Schaeffer and McDonald (1978); and *Semionotus* from Olsen and McCune (1991).

(~10‰ for the whole data set and more than 5‰ for the Silver Ridge B-1 core) than those at the ETE, far more frequent than reasonable, and largely tracked lacustrine facies. This led to the conclusion that mixing between multiple organic carbon sources with different characteristic $\delta^{13}C$ values was responsible for the large shifts, and that the $\delta^{13}C_{org}$ record might be more useful as a proxy of lacustrine ecosystem function than atmospheric composition.

The section sampled by the Silver Ridge B-1 core is particularly informative because it directly overlies the first Hartford basin CAMP basalt and should be very close in time to the end-Triassic extinction. The data indicate that the cyclicity it records is unusual compared to the pattern seen in other parts of the Hartford basin section and in the neighboring Newark basin where the cyclicity has been documented in detail (e.g., Olsen and Kent, 1996). Specifically, the Silver Ridge B-1 core cyclicity is more complicated than typical Van Houten cycles, which are very easily picked out by eye and whose thicknesses look periodic. The stratal patterns in core B-1, lend itself well to the typological approach to identify the Van Houten cycles, and a more jaundiced eye might even conclude that the cycle pattern in the Silver Ridge B-1 core is aperiodic. However, Fourier analysis reveals periodicities that are relatively strong and a simple age model for these strata shows that there is a strong half-precessional (~10 ky) signal as well as the usual climatic precessional cycle of ~20 ky (Fig. 13), which is significant for understanding the effect of the CAMP eruptions.

For the simple age model the 17 m depth rank cycle is assumed to be a Van Houten cycle corresponding to the 20 ky climatic precession cycle. The ~112 m cycle would thus have a period of ~132 ky, close to the 125 ky eccentricity cycle (given the poor spectral precision for this cycle), and the various cycles near 10 m would have a period of 12 ky. The depth rank, color, and TOC cycles with a thickness period of ~11 m would have a period of ~13 ky and the cycles in $\delta^{13}C_{org}$ with thickness periods of 9.8 and 8.4 m would correspond to periods of 11.3 and 9.6 ky, respectively. The fact that most of the variance in the original complex $\delta^{13}C_{org}$ is captured by these frequencies (Figs. 7 and 13) strongly suggests the climatic periodicities have been correctly identified, and Blackburn et al. (2009) provide new U–Pb dates from eastern North America consistent with this age model.

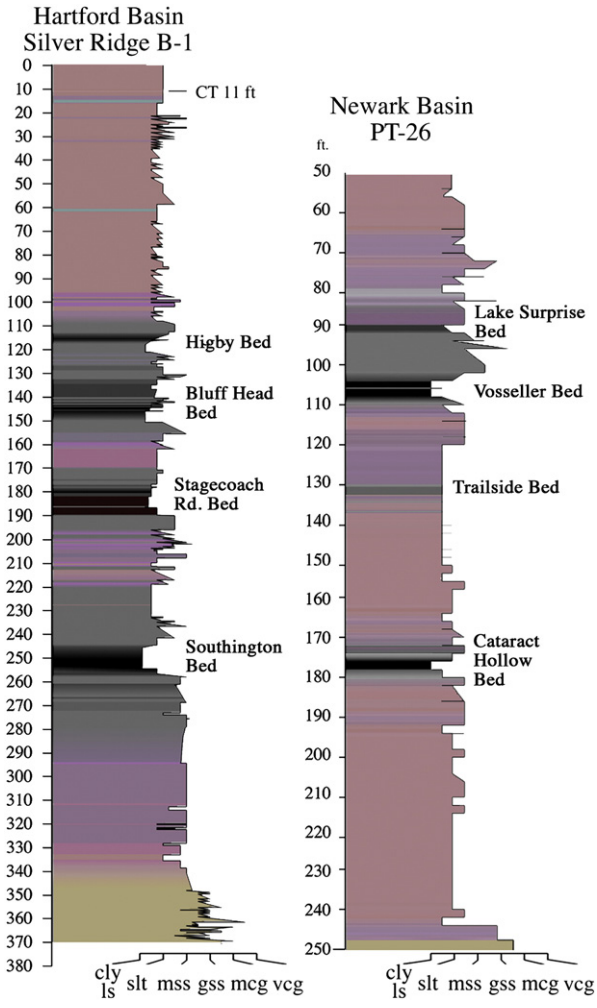

Fig. 16. Comparision of the stratigraphy of the lower Shuttle Meadow of the Hartford basin based on the Silver Ridge B-1 core and the lower Feltville Formation of the Newark basin based on the Army Corps of Engineers PT-26 (housed at the core repository of Rutgers University). Modified from Olsen (2010).

The cyclostratigraphy of Silver Ridge B-1 core and the Shuttle Meadow Formation is exceedingly similar to that of the Feltville Formation of the Newark basin (Olsen, 2010; Whiteside et al., 2007) down to details of the individual cycles and sub-cycles (Fig. 16), suggesting they were controlled by the same processes, such as climate change, or were part of the same lake, which are not mutually exclusive options. The possibility that the lakes of the Hartford and Newark basin were connected during at least high stands is reinforced by the similarity between not only the details of stratigraphy of the Shuttle Meadow and Feltville formations of the Hartford and Newark basins, but also the similarities with the stratigraphy of the lower Cass Formation (LeTourneau and Huber, 2006) of the Pomperaug basin in Connecticut and the Midland Formation of the Culpeper basin of Virginia. These similarities extend not only to the basic stratigraphy of the units but also to the fish assemblages. If the Shuttle Meadow lakes extended during highstands all the way to Virginia, the lakes would be larger in area than lakes Tanganyika and Malawi and would be among the largest lakes known (Fig. 2). However, the fact that these lakes dried out completely during low stands indicates they probably were never as deep as the latter two modern lakes.

Thus, the fluctuations in $\delta^{13}C_{org}$ record climate change via water depth. It appears that this occurs because ecosystem function is controlled by water depth, causing differential preservation to be more important to the final $\delta^{13}C_{org}$ values than changes in input or changes in the isotopic composition of atmospheric CO_2.

Preservation of organic material is intimately related to precipitation and hence water depth because of the effect of depth on turbulent stratification of the water column and therefore oxygen distribution (Olsen, 1990). It is hypothesized that in shallow water, regardless of the levels of autochthonous algal production, most of this $\delta^{13}C$-depleted labile material of phytoplankton origin was respired during wind-driven resuspension and bioturbation, leaving a residuum of recalcitrant vascular plant material relatively enriched in ^{13}C. Conversely, deposition in the deeper water intervals favors preservation of relatively ^{12}C enriched autochthonous material because of the shorter residence time of organic matter in the more metabolically active portions of the lake ecosystem. Because the ratio of the allochthonous (woody) to autochonous (phytoplankton) carbon was so high in shallow water portions of the Shuttle Meadow Formation, other effects were overwhelmed and the overall $\delta^{13}C_{org}$ curve of the Silver Ridge B-1 core reflects mostly the ecosystem effects of changing water depth. These processes can be conceptualized in a simple mixing model in which the ratios of the vascular plant vs. phytoplankton/bacteria end-members are controlled largely by differential preservation and a lesser component of control by the biological pump (Fig. 17).

Support for this hypothesis comes from Spiker et al. (1988) and Pratt et al. (1986, 1988) who demonstrate that autochthonous-derived kerogens from the Bluff Head and Southington beds are depleted (−27‰ to −29‰) in ^{13}C compared to phytoclasts from the same bed (−23‰ and −25‰); these values are comparable to the −24‰ and −26‰ of $\delta^{13}C_{org}$ seen in red and light gray beds. This same pattern is seen in the difference between the $\delta^{13}C_{org}$ data and wood data (Fig. 7). The $\delta^{13}C_{org}$ of vascular plant material reflects the isotopic composition of atmospheric CO_2 with a characteristic fractionation (Farquhar et al., 1980, 1989). Fluctuations in the latter are due to changes in the global carbon cycle, some aspects of which may vary with Milankovitch processes operating on the surface oceanic carbon reservoirs and/or rare events such as those associated with mass extinctions.

Some of the most ^{13}C-depleted $\delta^{13}C_{org}$ values may result from a contribution of organic matter from methanotrophic bacteria ($\delta^{13}C$ typically −58.1‰; Whiticar and Faber, 1985). Because lake waters

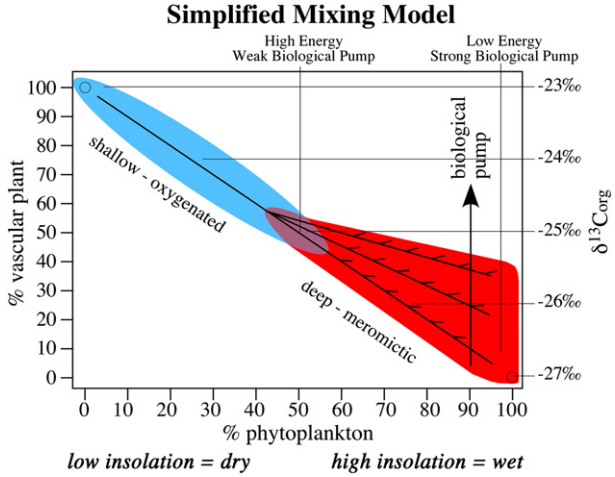

Fig. 17. Conceptual model of the mixing relationship between carbon of different sources with distinctive $\delta^{13}C$ values controlled by lake depth, and hence climate. This is simplified mixing diagram assuming a vascular plant-dominated end member preferentially preserved in very shallow lakes with a $\delta^{13}C$ value of −23‰, and a phytoplankton-dominated end member of −27‰, preferentially preserved in the meromictic, deep water lake stage. Increasing lake depth increases the stability of chemical stratification leading to greater preservation of labile phytoplankton and plant cuticular material leading to more negative values for the bulk organic $\delta^{13}C$, but stable meromixis leads to a more efficient biological pump (arrow and ticks on mixing line) driving the $\delta^{13}C$ towards more positive values.

tend to be less enriched in sulfate than marine waters (Berner and Raiswell, 1983), methanogenesis may have been enhanced by stable stratification in deeper stages of the lake, especially when sulfate was low.

Another possibility is that atmospheric carbon isotope ratios were changing drastically and could contribute to the variance within a cycle. This hypothesis suggests that these fluctuations were not due to fluctuations in the global atmospheric/surface oceanic carbon reservoir by examining the carbon isotopic component of long-chain normal hydrocarbons (*n*-alkanes) derived from vascular plant cuticular waxes (Figs. 7 and 14). A sample was selected from the deep-water Bluff Head Bed in the Silver Ridge core in which the $\delta^{13}C_{org}$ values are relatively ^{13}C depleted [−27.07‰ at 44.58 m (146.25 ft)] and a sample from a shallow water unit that exhibits relative a ^{13}C enriched value [−24.78‰ at 42.291 m (138.75 ft)]. The odd C_{25}–C_{31} *n*-alkanes from these samples show only very small differences (−29.93‰ to −30.44‰, respectively) compared to the bulk organic carbon values, with the shallow water unit having the most ^{13}C-depleted value. This suggests relatively little atmospheric contribution to the variance within at least this cycle, and if the plant wax *n*-alkanes are faithfully recording atmospheric $\delta^{13}C$, what contribution there is shifts the values depleted in ^{13}C in the opposite direction to what is seen in the bulk data for the same samples (Fig. 14).

Some cheirolepidaceous conifers have been suggested to have had C_4 metabolisms (Bocherens et al., 1994), and these conifers are the most common fossils in the Shuttle Meadow Formation. The change in $\delta^{13}C$ values from deep (wet) to shallow (dry) environments is in the right direction, so it might be argued that at least some of the variability could be due to variable contributions from C_4 plants as has been observed in modern lakes (Feakins et al., 2005; Talbot and Johannessen, 1992). However, this experiment comparing *n*-alkanes from the wet and dry environments shows that the variability in $\delta^{13}C_{org}$ cannot be easily attributable to C_4 plants, because they should be more prevalent in the drier environments, yet, as shown above, the shallower water (i.e. drier) interval has more ^{13}C-depleted *n*-alkane values than the deeper water (wetter) intervals.

Hence, it can be concluded that fluctuations in the bulk $\delta^{13}C_{org}$ of the cyclical Shuttle Meadow Formation strata are at the scale of a single deeper water unit, largely a function of the burial efficiency of the autochthonous carbon, itself a function of lake meromixis, encouraged by increasing water depth and relatively high levels of organic productivity. At larger scales, the carbon isotopes record the differential mixing of kerogen sources due to the degree of stratification of the lake. The three most negative $\delta^{13}C_{org}$ values (~−29‰) occur in the deepest water units, reflecting a dominance of phytoplankton and bacteria over vascular-plant-derived organic matter, possibly augmented by methanogenic contributions (Fig. 17). This mixing model is different than mixing models often used for unraveling the $\delta^{13}C$ history of lacustrine deposits (e.g., Stephenson et al., 2006; Scholz et al., 2003; Mayr et al., 2009) because in the latter, only changes in the source inputs, not differential preservation, are considered.

Fourier analysis and the simple age model used here show that the most prominent periods in Silver Ridge Core lithology, relative water depth, and $\delta^{13}C$ time are 20 ky, and surprisingly, cycles at about half that period: 13 to 10 ky. Milankovitch insolation theory predicts that half precession cyclicity will be dominant at the equator if the climate or depositional system is sensitive to the time of maximum insolation (solar radiation energy received on a given surface area in a given time) independent of the calendar day (Berger et al., 2006; Short et al., 1991), but direct local forcing should fade away by 5°N. Thus, evidence for expression of the half precession cycle as far north as the Shuttle Meadow Formation (~21°N paleolatitude) is not expected. This climate signal was likely exported to areas far away from the equator, possibly via El Niño-like processes (cf. Huber and Caballero, 2003; Ripepe et al., 1991; Trauth et al., 2003; Turney et al., 2004). Equatorial climate variations would be expected to be sensitive to the time of maximum insolation to be more efficiently communicated to higher latitudes during a time of anomalous warmth, such as that hypothesized to be caused by CAMP-related greenhouse gases with a concomitant intensification in the hydrological cycle (e.g., Bonis et al., 2010).

A striking aspect of the lower Shuttle Meadow Formation is the prevalence of limestones, a feature shared with all of the units above and interbedded with the initial CAMP basalts in eastern North America and Morocco. This prevalence of limestone is unusual in this context because limestones are otherwise rare in strata above, below and interbedded with later CAMP flows. One exception is the basal East Berlin Formation in the Hartford basin (Figs. 3 and 4), resting on the Holyoke Basalt, which has a locally well-developed limestone sequence (Starquist, 1943), but in other areas none of the later basalts have associated limestones. Although an attractive hypothesis for the abundant lower Shuttle Meadow Formation limestones might simply be a carbonation reaction in basalt weathering yielding lacustrine limestone as the final product, the nearly complete absence of limestones above other basalts in eastern North America and Morocco argues against the production of these limestones being controlled by the availability of weathered basalt alone.

A related phenomenon in the basal Shuttle Meadow Formation is the apparent conversion of Talcott Formation basalt volcanoclastics, largely breccia, to limestone and calcareous mudstone that still preserve igneous textures, in the Totoket fault block near the Bluff Head locality (Steinen et al., 1987). Nearby, there are carbonate "algal reefs" and associated limestone in the basal Shuttle Meadow Formation which have been interpreted as a hot spring deposit, but seem in keeping with the general carbonate-rich nature of the formation (DeWet et al., 2002; Krynine, 1950; Mooney, 1979; Steinen et al., 1987).

It seems plausible that the interval of time represented by the lower Shuttle Meadow Formation was characterized by an anomalously high frequency of limestone deposition, compared to other strata in the same tectonic context, because of *both* the high levels of atmospheric CO_2 driving especially vigorous weathering and carbonation of the basalt and an intensified hydrological cycle (e.g. Whiteside et al., 2010). Thus, the unusual characteristics of the succession are all explained by the same phenomenon: a transient and dramatic increase in CO_2 caused by the initial CAMP eruptions.

Although data from eastern North America show most extinctions at the pulse below the locally oldest CAMP basalts, it is clear that elsewhere, especially at high latitudes (>30°N), extinctions continued, and some major groups such as conodonts and some pollen taxa such as *Rhaetipollis* do not have their last occurrences until well into Shuttle Meadow time (Cirilli et al., 2009; Whiteside et al., 2010). The same is true of the plant extinctions described by McElwain et al. (2007, 2009) from East Greenland. This suggests that the lower Shuttle Meadow Formation was deposited during a time of major global ecological stress. The most abundant pollen taxon in the Shuttle Meadow Formation, the cheirolepidiaceous conifer *Classopollis meyeriana* (Cornet and Traverse, 1975), increases in abundance (>90%) dramatically at the extinction level and does not decline in abundance until after the CAMP episode (Cornet, 1977). Relatively abundant megafossils of the dipteridaceous fern *Clathropteris meniscoides* occur in the Shuttle Meadow Formation and its correlatives in eastern North America, whereas it its virtually absent elsewhere except just above the extinction level below the oldest basalt. Together, *Classopollis meyeriana* and *Clathropteris meniscoides* appear to be disaster taxa dominant during the episode of high CO_2 and ecosystem stress.

6. Conclusions

Ecosystem structure is often discussed in terms of the evolution of complex interactions though a continuum of environments and lineages. However, lacustrine ecosystems are discontinuous water islands in a sea of land and the degree to which ecosystem structure

and function are peculiar to the specific history of an individual lake is not well understood. As relatively confined areas and hence perhaps more easily understood as an experimental system, Forbes' (1887) concept of "The lake as a microcosm" derived from comparisons in space, can be extended to comparisons through time. This concept has been explored here, not by looking at a series of lakes through time in the same space, but by looking at the record of ecosystem processes in fossil lakes via carbon dynamics and assemblages of fish taxa, in which the geographic context of the lakes remains constant, but water depth, the major control of lacustrine ecosystems within individual basins, is in cyclical flux. However, the particular lake sequence examined here was deposited during an exceptional time, cycling through both the eruption of one of the largest flood basalt provinces of all time, the CAMP, and the end Triassic mass extinction.

As seen in the Bluff Head data sets, *Semionotus* is most abundant during intervals spanning the rise (cycle W-6, Bluff Head Bed) and fall of individual high-stand deposits of a Van Houten cycle (Bluff Head Bed). *Redfieldius* was more abundant during maximum lake level when a carbonate-rich laminite was deposited and the biological pump was strengthened by meromixis. The higher-level fish taxa were sorted by extrinsic environmental change, but intrinsic factors within *Semionotus* governed the evolution of a species flock once great lakes were established in the rifts during the initial phases of the CAMP eruption.

Our $\delta^{13}C$ data show a remarkable fidelity to the hierarchical patterns of Milankovitch forcing, and lacustrine ecosystem carbon dynamics responded to the extrinsic forcing of climate in predictable and cyclical ways, reflecting differential preservation of vascular plant matter during lake low stands and phytoplankton and bacterial biomass during lake high-stands. During high-stands the efficacy of the biological pump was controlled by lake stratification. Fish taxa were filtered by the lake wet and dry cycles, chemistry, and stratification patterns. The evolution of the fishes through individual cycles produced a myriad of species, adding up to no apparent net change on the long term as the lake dried up. This deep time extension of Forbes' concept suggests that such patterns might be widespread ecosystem properties made obvious by the very tangible boundaries of lakes, but also inherent to other less physically prescribed systems, even when they occur in times of exceptional change.

Acknowledgements

We thank Raymond Sambrotto for assistance with mass spectrometry and use of his lab at LDEO, Daniel Montluçon and Carl Johnson for their skilled assistance in processing $\delta^{13}C$ samples, and Jay Ague and Matthew Whiteside for technical support. Peter LeTourneau was a co-investigator on the Silver Ridge cores and was instrumental in their siting and recovery. This research was aided by a National Science Foundation Graduate Research Fellowship, a Grants In Aid of Research from Sigma Xi, The Scientific Research Society, and by the Department of Earth and Environmental Sciences at Columbia University to Whiteside, and grants from the National Science Foundation to Olsen (EAR-0753496) and to D.V. Kent and Olsen (EAR-0446843 and EAR-0000922). Permission from the Nature Conservancy to conduct excavations in the Bluff Head Bed is gratefully acknowledged, as well as permission from the developers of the Silver Ridge community to conduct geological investigations on the construction sites. We especially highlight helpful comments from Mark V.H. Wilson, Finn Surlyk, and an anonymous reviewer for many suggestions that greatly improved the paper. This is a contribution to IGCP Projects 458 and 506 as well as an LDEO contribution number 7428.

Appendix A. Supplementary data

Supplementary data to this article can be found online at doi:10.1016/j.palaeo.2010.11.025.

References

Anderson, R.Y., Dean, W.E., 1988. Lacustrine varve formation through time. Palaeogeography, Palaeoclimatology, Palaeoecology 62, 215–235.
Benton, M.J., 1995. Diversification and extinction in the history of life. Science 268, 52–58.
Berger, A.L., Loutre, M.F., Dehant, V., 1989. Influence of the changing lunar orbit on the astronomic frequencies of the Pre-Quaternary insolation patterns. Paleoceanography 4, 555–564.
Berger, A., Loutre, M.F., Mélice, J.L., 2006. Equatorial insolation: from precession harmonics to eccentricity frequencies. Climates of the Past 2, 131–136.
Berner, R.A., Raiswell, R.A., 1983. Burial of organic carbon and pyrite sulfur in sediments over Phanerozoic time. A new theory. Geochimica et Cosmochimica Acta 28, 855–862.
Blackburn, T., Bowring, S., Olsen, P., Kent, D., Rasburym, T., McHone, G., 2009. U–Pb zircon dating of Central Atlantic Magmatic Province: implication for the Triassic–Jurassic extinction and the astrochronological timescale. Geological Society of America Abstracts with Programs 41 (7), 421.
Bocherens, H., Friis, E.M., Mariotti, A., Pedersen, K.R., 1994. Carbon isotopic abundances in Mesozoic and Cenozoic fossil plants: palaeoecological implications. Lethaia 26, 347–358.
Bogen, A.N., Wilson, M.V.H., 1994. Tests of the annual hypothesis and temporal calibration of a 6375-varve fish-bearing interval, Eocene Horsefly Beds, British Columbia, Canada. Historical Biology 7, 325–339.
Bonis, N.R., Ruhl, M., Kurschner, W.M., 2010. Climate change driven black shale deposition during the end-Triassic in the western Tethys. Palaeogeography, Palaeoclimatology, Palaeoecology 290, 151–159.
Cirilli, S., Marzoli, A., Tanner, L., Bertrand, H., Buratti, N., Jourdan, F., Bellieni, G., Kontak, D., Renne, P.R., 2009. Latest Triassic onset of the Central Atlantic Magmatic Province (CAMP) volcanism in the Fundy Basin (Nova Scotia): new stratigraphic constraints. Earth and Planetary Science Letters 286, 514–525.
Color, Munsell, 2009. Geological Rock Color Chart. Munsell Color, Grand Rapids, MI. 9 pp.
Cooper, M.C., O'Sullivan, P.E., Shine, A.J., 2000. Climate and solar variability recorded in Holocene laminated sediments—a preliminary assessment. Quaternary International 68, 363–371.
Cornet, B., 1977. The Palynostratigraphy and Age of the Newark Supergroup. Ph.D thesis, The Pennsylvania State University, State College, PA, 504 pp.
Cornet, B., 2001. Massive Ancient Fish Kills: Nature's Pollution. http://www.sunstar-solutions.com/sunstar/BluffHead/bluffhead.htm.
Cornet, B., Traverse, A., 1975. Palynological contribution to the chronology and stratigraphy of the Hartford Basin in Connecticut and Massachusetts. Geoscience and Man 11, 1–33.
Cornet, W.B., Traverse, A., McDonald, N.G., 1973. Fossil spores, pollen, and fishes from Connecticut Indicate Early Jurassic Age for Part of the Newark Group. Science 182, 1243–1247.
Davis, W.M., Loper, S.W., 1891. Two belts of fossiliferous black shale in the Triassic Formation of Connecticut. Geological Society of America, Bulletin 2, 415–430.
Dean, W.E., 2006. The geochemical record of the last 17,000 years in the Guaymas Basin, Gulf of California. Chemical Geology 232, 87–98.
Dean, J.M., Kemp, A.E.S., Bull, D., Pike, J., Patterson, G., Zolitschka, B., 1999. Taking varves to bits: scanning electron microscopy in the study of laminated sediments and varves. Journal of Paleolimnology 22, 121–136.
DeWet, C.B., Mora, C.I., Gore, P.J.W., Gierlowshi-Kordesch, E., Cucolo, S.J., 2002. Deposition and geochemistry of lacustrine and spring carbonates in Mesozoic rift basins, eastern North America. In: Renaut, R.W., Ashley, G.M. (Eds.), Sedimentation in Continental Rifts: SEPM Special Publication No. 73, pp. 309–325.
Dickneider, T.A., Ellen Murphy, S.M., Sallavanti, R.A., Stephens, K., 2003. In: LeTourneau, P.M., Olsen, P.E. (Eds.), Organic geochemistry of lacustrine shales of the Shuttle Meadow and Portland formations of the Hartford basin, Newark Supergroup, Connecticut: The Great Rift Valleys of Pangea in Eastern North America, vol. 2, pp. 123–140.
Espie, G.S., Miller, A.G., Kandasamy, R.A., Canvin, D.T., 1991. Active HCO_3^- transport in cyanobacteria. Canadian Journal of Botany 69, 936–944.
Farquhar, G.D., von Caemmerer, S., Berry, J.A., 1980. A biochemical model of photosynthetic CO_2 assimilation in leaves of C_3 plants. Planta 149, 78–90.
Farquhar, G.D., Ehleringer, Hubick, K.T., 1989. Carbon isotope discrimination and photosynthesis. Annual Review of Plant Physiology and Plant Molecular Biology 40, 503–538.
Feakins, S., deMenocal, P., Eglington, T., 2005. Biomarker records of Late Neogene Changes in East African Vegetation. Geology 33, 977–980.
Forbes, S.A., 1887. The lake as a microcosm. Bulletin of the Scientific Association (Peoria, IL) 1887, 77–87.
Forel, F.A., 1885. Le ravin sous-lacoustre des fleuves glaciaires. Comptes Rendus de l'Académie des sciences, Paris 101, 725–728.
Fowell, S.J., Olsen, P.E., 1993. Time-calibration of Triassic/Jurassic micro-floral turnover, eastern North America. Tectonophysics 222, 361–369.
Fowell, S.J., Traverse, A., 1995. Palynology and age of the upper Blomidon Formation, Fundy Basin, Nova Scotia. Review of Palaeobotany and Palynology 86 (3–4), 211–233.
Gilfillian, A.M., Olsen, P.E., 2000. The coelacanth *Diplurus longicaudatus* as the origin of the large coprolites occurring in the Triassic–Jurassic lacustrine strata of Eastern North America. Geological Society of America, Abstracts with Programs 32 (1), A-20.
Hesselbo, S.P., Robinson, S.A., Surlyk, F., Piasecki, S., 2002. Terrestrial and marine extinction at the Triassic–Jurassic boundary synchronized with major carbon-cycle perturbation: a link to initiation of massive volcanism? Geology 30, 251–254.
Hillebrandt, A.v., Krystyn, L., Kuerschner, W.M., Bown, P.R., McRoberts, C., Ruhl, M., Simms, M., Tomasovych, A., Urlichs, M., 2007. A candidate GSSP for the base of the Jurassic in the Northern Calcareous Alps (Kuhjoch section, Karwendel Mountains,

Tyrol, Austria). International Subcommission on Jurassic Stratigraphy, Newsletter 34 (1), 2–20.
Holser, W.T., Magaritz, M., 1987. Events near the Permian–Triassic boundary. Modern Geology 11, 155–180.
Hsü, K.J., McKenzie, J.A., He, Q.X., 1982. Terminal Cretaceous environmental and evolutionary changes. In: Silver, L.T., Schultz, P.H. (Eds.), Geological Implications of Impacts of Large Asteroids and Comets on the Earth: Geological Society of America Special Paper, 190, pp. 317–328.
Huber, M., Caballero, R., 2003. Eocene El Nino: evidence for robust tropical dynamics in the "hothouse". Science 299, 877–881.
Hubert, J.F., Reed, A.A., Carey, P.J., 1976. Paleogeography of the East Berlin Formation, Newark Group, Connecticut Valley. American Journal of Science 276, 1183–1207.
Johnson, T.C., 1984. Sedimentation in large lakes. Annual Review of Earth and Planetary Science 12, 179–204.
Karner, G.D., Byamungu, B.R., Ebinger, C.J., Kampunzu, A.B., Mukasa, R.K., Nyakaana, J., Rubondo, E.N.T., Upcott, N.M., 2000. Distribution of crustal extension and regional basin architecture of the Albertine rift system, East Africa. Marine and Petroleum Geology 17, 1131–1150.
Kent, D.V., Olsen, P.E., 2000. Magnetic polarity stratigraphy and paleolatitude of the Triassic–Jurassic Blomidon Formation in the Fundy basin (Canada): implications for early Mesozoic tropical climate gradients. Earth and Planetary Science Letters 179, 311–324.
Kent, D.V., Olsen, P.E., 2008. Early Jurassic magnetostratigraphy and paleolatitudes from the Hartford continental rift basin (eastern North America): testing for polarity bias and abrupt polar wander in association with the central Atlantic magmatic province. Journal of Geophysical Research 113, B06105. doi:10.1029/2007JB005407.
Kent, D.V., Tauxe, L., 2005. Corrected Late Triassic latitudes for continents adjacent to the North Atlantic. Science 307, 240–244.
Kent, D.V., Olsen, P.E., Witte, W.K., 1995. Late Triassic–Early Jurassic geomagnetic polarity and paleolatitudes from drill cores in the Newark rift basin (Eastern North America). Journal of Geophysical Research 100 (B8), 14,965–14,998.
Kriwet, J., 2001. Feeding mechanisms and ecology of pycnodont fishes (Neopterygii, †Pycnodontiformes). Mitteilungen aus dem Museum für Naturkunde in Berlin. Geowissenschaftliche Reihe 4, 139–165.
Krynine, P.D., 1950. Petrology, stratigraphy and origin of the Triassic sedimentary rocks of Connecticut. Connecticut Geology and Natural History Survey Bulletin 73, 247.
Lauder, G.V., 1980. In: Schneck, D. (Ed.), Hydrodynamics of prey capture by teleost fishes. : Biofluid Mechanics, 11. Plenum Press, New York, pp. 161–181.
Lauder, G.V., 1982. Patterns of evolution in the feeding mechanism of actinopterygian fishes. American Zoologist 22, 275–285.
LeTourneau, P.M., Huber, P., 2006. Early Jurassic eolian dune field, Pomperaug basin, Connecticut and related synrift deposits: stratigraphic framework and paleoclimatic context. Sedimentary Geology 187, 63–81.
Marzoli, A., Renne, P.R., Piccirillo, E.M., Ernesto, M., Bellieni, G., De Min, A., 1999. Extensive 200-million-year-old continental flood basalts of the Central Atlantic magmatic province. Science 284, 616–618.
Marzoli, A., Bertrand, H., Knight, K.B., Cirilli, S., Buratti, N., Vérati, C., Nomade, S., Renne, P.R., Youbi, N., Martini, R., Allenbach, K., Neuwerth, R., Rapaille, C., Zaninetti, L., Bellieni, G., 2004. Synchrony of the Central Atlantic magmatic province and the Triassic–Jurassic boundary climatic and biotic crisis. Geology 32, 973–976.
Mattinson, J.M., 2005. Zircon U–Pb chemical abrasion ("CA-TIMS") method: combined annealing and multi-step partial dissolution analysis for improved precision and accuracy of zircon ages. Chemical Geology 220, 47–66.
Mayr, C., Andreas Lücke, A., Nora, I., Maidana, N.I., Michael Wille, M., Haberzettl, T., Corbella, H., Ohlendorf, C., Schäbitz, F., Fey, M., Janssen, S., Zolitschka, B., 2009. Isotopic fingerprints on lacustrine organic matter from Laguna Potrok Aike (southern Patagonia, Argentina) reflect environmental changes during the last 16,000 years. Journal of Paleolimnology 42, 81–102.
McCune, A.R., 1981. Quantitative description of body form in fishes: implications for species level taxonomy and ecological inference. Copeia 4, 897–901.
McCune, A.R., 1990. Morphological anomalies in the *Semionotus* complex: relaxed selection during colonization of an expanding lake. Evolution 44, 71–85.
McCune, A.R., Thomson, K.S., Olsen, P.E., 1984. Semionotid fishes from the Mesozoic Great Lakes of North America. In: Echelle, A.A., Kornfield, I. (Eds.), Evolution of Species Flocks. University of Maine at Orono Press, Orono, pp. 27–44.
McDonald, N.G., 1975. Fossil Fishes from the Newark Group of the Connecticut Valley. Unpul. Masters Thesis, Wesleyan University, 230 p.
McElwain, J.C., Popa, M.E., Hesselbo, S.P., Haworth, M., Surlyk, F., 2007. Macroecological responses of terrestrial vegetation to climatic and atmospheric change across the Triassic/Jurassic boundary in East Greenland. Paleobiology 33 (4), 547–573.
McElwain, J.C., Wagner, P.J., Hesselbo, S.P., 2009. Fossil plant relative abundances indicate sudden loss of Late Triassic biodiversity in East Greenland. Science 324, 1554–1556.
Mooney, J., 1979. The Origin and Diagenetic History of a Mesozoic Carbonate Hot Spring Deposit, Coe's Quarry, North Branford, Connecticut. M.Sc. Thesis, Department of Geology, University of Connecticut, Storrs, CT. 100 p.
Morton, N., 2008a. Selection and voting procedures for the base Hettangian. International Subcommission on Jurassic Stratigraphy, Newsletter 35 (1), 67.
Morton, N., 2008b. Details and voting procedures for the base Hettangian. International Subcommission on Jurassic Stratigraphy, Newsletter 35 (1), 74.
Morton, N., Warrington, G., Bloos, G., 2008. Forward. International Subcommission on Jurassic Stratigraphy, Newsletter 35, 68–73.
Mundil, R., Ludwig, K.R., Metcalfe, I., Renne, P.R., 2004. Age and timing of the Permian mass extinctions: U/Pb dating of closed-system zircons. Science 305, 1760–1763.
Olsen, P.E., 1980. Fossil great: lakes of the Newark Supergroup in New Jersey. In: Manspeizer, W. (Ed.), Field Studies in New Jersey Geology and Guide to Field Trips: 52nd Annual Meeting, New York State Geological Association, Newark College of Arts and Sciences, Newark, NJ, Rutgers University, pp. 352–398.
Olsen, P.E., 1986. A 40-million-year lake record of early Mesozoic orbital climatic forcing. Science 234, 842–848.
Olsen, P.E., 1990. Tectonic, climatic, and biotic modulation of lacustrine ecosystems: examples from the Newark Supergroup of eastern North America. In: Katz, B. (Ed.), Lacustrine Basin Exploration: Case Studies and Modern Analogs: American Association Petroleum Geologists Memoir, 50, pp. 209–224.
Olsen, P.E., 2010. Fossil great lakes of the Newark Supergroup—30 years later. In: Benimoff, A.I. (Ed.), Field Trip Guidebook, New York State Geological Association: 83nd Annual Meeting, College of Staten Island, pp. 101–162.
Olsen, P.E., Galton, P.M., 1977. Triassic–Jurassic tetrapod extinctions: are they real? Science 97, 983–986.
Olsen, P.E., Kent, D.V., 1996. Milankovitch climate forcing in the tropics of Pangea during the Late Triassic. Palaeogeography, Palaeoclimatology, Palaeoecology 122, 1–26.
Olsen, P.E., Kent, D.V., 1999. Long-period Milankovitch cycles from the Late Triassic and Early Jurassic of eastern North America and their implications for the calibration of the early Mesozoic time scale and the long-term behavior of the planets. Philosophical Transactions of the Royal Society A 357, 1761–1787.
Olsen, P.E., Kent, D.V. 2000. High-resolution early Mesozoic Pangean climatic transect in lacustrine environments. In Bachmann, G., Lerche, I. (Eds.), Epicontinental Triassic, vol 3, Zentralblatt fur Geologie und Palaontologie, VIII, pp. 1475–1496.
Olsen, P.E., McCune, A.R., 1991. Morphology of the *Semionotus elegans* species group from the Early Jurassic part of the Newark Supergroup of Eastern North America with comments on the family Semionotidae (Neopterygii). Journal of Vertebrate Paleontology 11 (3), 269–292.
Olsen, P.E., Whiteside, J.H., 2008. Pre-Quaternary Milankovitch cycles and climate variability. In: Gornitz, V. (Ed.), Encyclopedia of Paleoclimatology and Ancient Environments, Earth Science Series. Kluwer Academic Publishers, Dordrecht, the Netherlands, pp. 826–835.
Olsen, P.E., McCune, A.R., Thomson, K.S., 1982. Correlation of the early Mesozoic Newark Supergroup by Vertebrates, principally fishes. American Journal of Science 282, 1–44.
Olsen, P.E., Schlische, R.W., Fedosh, M.S., 1996a. 580 ky duration of the Early Jurassic flood basalt event in eastern North America estimated using Milankovitch cyclostratigraphy. In: Morales, M. (Ed.), The Continental Jurassic: Museum of Northern Arizona Bulletin, 60, pp. 11–22.
Olsen, P.E., Kent, D.V., Sues, H.-D., Koeberl, C., Huber, H., Montanari, A., Rainforth, E.C., Fowell, S.J., Szajna, M.J., Hartline, B.W., 2002. Ascent of dinosaurs linked to an iridium anomaly at the Triassic–Jurassic boundary. Science 296, 1305–1307.
Olsen, P.E., Kent, D.V., Et-Touhami, M., Puffer, J.H., 2003a. Cyclo-, magneto-, and biostratigraphic constraints on the duration of the CAMP event and its relationship to the Triassic–Jurassic boundary. In: Hames, W.E., McHone, J.G., Renne, P.R., Ruppel, C. (Eds.), The Central Atlantic Magmatic Province: Insights from Fragments of Pangea: Geophysical Monograph Series, vol. 136, pp. 7–32.
Olsen, P.E., Whiteside, J.H., Huber, P., 2003b. Causes and consequences of the Triassic-Jurassic mass extinction as seen from the Hartford basin. In: Brady, J.B., Cheney, J.T. (Eds.), Guidebook for Field Trips in the Five College Region, 95th New England Intercollegiate Geological Conference. Department of Geology, Smith College, Northampton, Massachusetts. B5-1–B5-41.
Olsen, P.E., Whiteside, J.H., LeTourneau, P.M., Huber, P., 2005. Jurassic cyclostratigraphy and paleontology of the Hartford basin. In: Skinner, B.J., Philpotts, A.R. (Eds.), 97th New England Intercollegiate Geological Conference. Department of Geology and Geophysics, Yale University, New Haven, Connecticut. pp. A4-1–A4-51.
Paillard, D., Labeyrie, L., Yiou, P., 1996. Macintosh program performs time-series analysis. EOS Transactions AGU 77, 379.
Patterson, C., 1973. In: Greenwood, P.H., Miles, R.S., Patterson, C. (Eds.), Interrelationships of holosteans. Interrelationships of Fishes. Academic Press, London, pp. 233–302.
Pettijohn, F.J., Potter, P.E., Siever, R., 1972. Sand and Sandstone. Springer-Verlag, New York. 618 pp.
Pratt, L.M., Vuletich, A.K., Shaw, C.A., 1986. Preliminary results of organic geochemical and stable isotope analyses of Newark Supergroup rocks in the Hartford and Newark basins. Eastern U.S. Geological Survey Open-File Report 86–284. 24 p.
Pratt, L.M., Shaw, C.A., Buruss, R.C., 1988. Thermal histories of the Hartford and Newark basins inferred from maturation indices of organic matter. In: Froelich, A.J., Robinson Jr., G.R. (Eds.), Studies of the Early Mesozoic Basins of the Eastern United States: U.S. Geological Survey Bulletin, 1776, pp. 58–62.
Puffer, J.H., 1992. Eastern North American flood basalts in the context of the incipient breakup of Pangaea. In: Puffer, J.H., Ragland, P.C. (Eds.), Eastern North American Mesozoic Magmatism: Geol. Soc. Am. Spec. Paper, 268, pp. 95–118.
Puffer, J.H., Hurtubise, D.O., Geiger, F.J., Lechler, P., 1981. Chemical composition and stratigraphic correlation of Mesozoic basalt units of the Newark Basin, New Jersey, and the Hartford Basin, Connecticut. Geological Society of America Bulletin 92, 155–159.
Redfield, W.C., 1841. Short notices of American fossil fishes. American Journal of Science, ser. 1 41, 24–28.
Ripepe, M., Roberts, L.T., Fischer, A.G., 1991. Enso and sunspot cycles in varved Eocene oil shales from image analysis. Journal of Sedimentary Research 61, 1155–1163.
Scandinavian Fishing Year Book ApS, 2009. *Engraulis japonicus*—Japanese anchovy [by Leenders, E.]. http://www.scandfish.com.
Schaeffer, B., 1948. A study of *Diplurus longicaudatus* with notes on the body form and locomotion of the Coelacantbini. American Museum Novitates 1378, 32.
Schaeffer, B., McDonald, N.G., 1978. Redfieldiid fishes from the Triassic–Liassic Newark Supergroup of Eastern North America. American Museum of Natural History Bulletin 159 (4), 131–173.

Schaeffer, B., Dunkle, D.H., McDonald, N.G., 1975. *Ptycholepis marshi* Newberry, a chondrostean Fish from the Newark Group of eastern North America. Fieldiana. Geology 33 (12), 205–233.
Schaltegger, U., Guex, J., Bartolini, A., Schoene, B., Ovtcharova, M., 2008. Precise U–Pb age constraints for end-Triassic mass extinction, its correlation to volcanism and Hettangian post-extinction recovery. Earth and Planetary Science Letters 267, 66–275.
Schoene, B., Crowley, J.L., Condon, D.J., Schmitz, M.D., Bowring, S.A., 2006. Reassessing the uranium decay constants for geochronology using ID-TIMS U–Pb data. Geochimica et Cosmochimica Acta 70, 426–445.
Schoene, B., Guex, J., Bartolini, A., Schaltegger, U., Blackburn, T.J., 2010. Correlating the end-Triassic mass extinction and flood basalt volcanism at the 100 ka level. Geology 38, 387–390.
Scholz, C.A., Rosenahl, B.R., 1988. Low lake stands in lakes Malawi and Tanganyika, East Africa, delineated with multifold seismic data. Science 240, 1645–1648.
Scholz, C.A., King, J.W., Ellis, G.S., Swart, P.K., Stager, J.C., Colman, S.M., 2003. Paleolimnology of Lake Tanganyika, East Africa, over the past 100 kyr. Journal of Paleolimnology 30, 139–150.
Seeley, H.G., 1886. Fresh-water Fishes of Europe: A History of Their Genera, Species, Structure, Habits, and Distribution. Cassell and Company, Limited, London.
Short, D.A., Mengel, J.G., Crowley, T.J., Hyde, W.T., North, G.R., 1991. Filtering of Milankovitch cycles by Earth's geography. Quaternary Research 35, 157–173.
Spiker, E.C., Kurt, R.K., Hatcher, P., Gottfried, R.M., Horan, M.F., Olsen, P.E., 1988. Source of kerogen in black shales from the Hartford and Newark basins, eastern U.S. In: Froelich, A.J., Robinson Jr., G.R. (Eds.), Studies of the Early Mesozoic Basins of the Eastern United States: U.S. Geological Survey Bulletin, 1776, pp. 63–68.
Starquist, V.L., 1943. The stratigraphy and structural geology of the central portion of the Mount Tom and East Mountain ridges. M.A. Thesis, Department of Geology, Smith College, Northampton, MA, p. 49.
Steinen, R.P., Gray, N.H., Mooney, J., 1987. A Mesozoic carbonate hot-spring deposit in the Hartford Basin of Connecticut. Journal of Sedimentary Petrology 57, 319–326.
Stephenson, M.H., Leng, M.J., Michie, U., Vane, C.H., 2006. Palaeolimnology of Palaeozoic lakes, focusing on a single lake cycle in the Middle Devonian of the Orcadian Basin, Scotland. Earth-Science Reviews 75, 177–197.
Talbot, M.R., Johannessen, T., 1992. A high resolution palaeoclimatic record for the last 27,500 years in tropical West Africa from the carbon and nitrogen isotopic composition of lacustrine organic matter. Earth and Planetary Science Letters 110, 23–37.
Trauth, M.H., Deino, A., Bergner, A.G.N., Strecker, M.R., 2003. East African climate change and orbital forcing during the last 175 kyr BP. Earth and Planetary Science Letters 206, 297–313.
Turney, C.S.M., Kershaw, A.P., Clemens, S.C., Branch, N., Moss, P.T., Fifield, L.K., 2004. Millennial and orbital variations of El Nino/Southern oscillation and high-latitude climate in the last glacial period. Nature 428, 306–310.
Van Houten, F.B., 1964. Cyclic lacustrine sedimentation, Upper Triassic Lockatong Formation, central New Jersey and adjacent Pennsylvania. In: Mermaid, O.F. (Ed.), Symposium on Cyclic Sedimentation: Kansas Geological Survey Bulletin, 169, pp. 497–531.
Vuorio, K., Meili, M., Sarvala, J., 2006. Taxon-specific variation in the stable isotopic signatures ($\delta^{13}C$ and $\delta^{15}N$) of lake phytoplankton. Freshwater Biology 51, 807–822.
Whiteside, J.H., 2006. Catastrophic, Climatic, and Biotic Modulation of Ecosystem Evolution. Ph.D. thesis, Department of Earth and Environmental Sciences, Columbia University, New York, NY, p. 220.
Whiteside, J.H., Olsen, P.E., Sambrotto, R.N., 2003. Negative $\delta^{13}C$ carbon isotopic anomaly in continental strata at the Triassic–Jurassic boundary in eastern North America (Newark Basin, Pennsylvania, USA). Geological Society of America, Abstracts with Programs 34 (7), 160.
Whiteside, J.H., Olsen, P.E., Kent, D.V., Fowell, S.J., Et-Touhami, M., 2007. Synchrony between the CAMP and the Triassic–Jurassic mass-extinction event? Palaeogeography, Palaeoclimatology, Palaeoecology 244, 345–367.
Whiteside, J.H., Olsen, P.E., Eglinton, T., Brookfield, M.E., Sambrotto, R.N., 2010. Compound-specific carbon isotopes from Earth's largest flood basalt eruptions directly linked to the end-Triassic mass extinction. Proceedings of the National Academy of Sciences 107, 6721–6725.
Whiticar, M.J., Faber, E., 1985. Methane oxidation in sediment and water column environments—isotope evidence. Advance Organic Geochemistry 10, 759–768.

1. Silver Ridge B-1 Core

depth ft	depth m	color	grain size	depth rank	TOC %	δ13C
-27.00	-8.23	2	1		0.5752	-27.31
11.00	3.35	0	2	1.5		
13.00	3.96	0	2	1.5		
13.01	3.97	0.5	2	1		
13.40	4.08	0.5	2	1	0.1875	-25.69
13.65	4.16	0.5	2	1	0.0582	-25.53
15.00	4.57	0.5	2	1		
15.01	4.58	0.75	2	1.5		
16.10	4.91	0.75	2	1.5		
16.11	4.91	0	1.5	1		
19.30	5.88	0	1.5	1	0.0458	-25.94
21.20	6.46	0	1.5	1		
21.21	6.46	0	3.5	1		
21.30	6.49	0	3.5	1		
21.31	6.50	0	1	1		
21.40	6.52	0	1	1		
21.41	6.53	0	3.5	1		
21.50	6.55	0	3.5	1		
21.51	6.56	0	1	1		
22.20	6.77	0	2	1		
22.21	6.77	0.25	4	1		
22.70	6.92	0.25	4	1		
22.71	6.92	0	1	1		
24.30	7.41	0	3	1		
24.31	7.41	0	2.5	1		
24.90	7.59	0	2.5	1		
24.91	7.59	0	1	1		
25.35	7.73	0	1.5	1	0.0463	-25.02
25.70	7.83	0	2	1		
25.71	7.84	0	1.5	1		
26.00	7.92	0	1.5	1		
26.01	7.93	0	4	1		
26.55	8.09	0	4	1		
26.56	8.10	0	1	1.25		
28.30	8.63	0	3	1.25		
28.31	8.63	0	1	1.25		
29.40	8.96	0	2	1.25	0.0470	-25.61
30.20	9.20	0	3	1.25		
30.21	9.21	0	1	1.25		
31.10	9.48	0	3	1.25		
31.11	9.48	0	1	0.5		

1. Silver Ridge B-1 Core

depth ft	depth m	color	grain size	depth rank	TOC %	δ13C
31.30	9.54	0	1	0.5	0.0456	-27.02
32.50	9.91	0.25	2	0.5		
32.51	9.91	0	1	0.5		
33.50	10.21	0	2	0.5		
33.51	10.21	0	1	0		
34.50	10.52	0	2	0		
34.51	10.52	0	1	0		
35.30	10.76	0	1.75	0		
35.31	10.76	0	1	0		
36.40	11.09	0	1.25	0.5	0.0619	-25.68
39.30	11.98	0	1.75	0.5		
39.31	11.98	0	1	0		
41.10	12.53	0	1	0		
41.11	12.53	0	1	0		
41.50	12.65	0	1.5	0	0.0523	-25.84
41.90	12.77	0	2	0		
41.91	12.77	0	1	0.25		
43.80	13.35	0	2	0.25		
43.81	13.35	0	1	0.5		
44.20	13.47	0	1	0.5		
44.21	13.48	0	1	0		
46.15	14.07	0	1.5	0	0.0491	-26.20
47.50	14.48	0	2	0		
47.51	14.48	0	1	0.25		
50.10	15.27	0	2	0.25		
50.11	15.27	0	2	0.25		
52.60	16.03	0	2	0.25	0.0546	-25.34
53.90	16.43	0	2	0.25		
53.91	16.43	0	2	0		
58.70	17.89	0	3	0		
58.71	17.89	0	1.5	1		
60.50	18.44	0	1.5	0.5	0.0953	-25.25
61.00	18.59	0	1.5	0.5		
61.01	18.60	0.5	1.5	1.5		
62.00	18.90	0.5	1.5	1.5		
62.01	18.90	0	1.5	1		
65.54	19.98	0	1.5	1	0.0420	-26.10
65.90	20.09	0	1.5	1		
65.91	20.09	0	1	1.5		
67.00	20.42	0	2	1.5		
67.01	20.42	0	1	1.5		

1. Silver Ridge B-1 Core

depth ft	depth m	color	grain size	depth rank	TOC %	δ13C
71.10	21.67	0	2	1.5		
71.11	21.67	0	1.5	1.75		
73.10	22.28	0	2	1.75		
73.11	22.28	0	1.5	1.5		
73.25	22.33	0	1.75	1.5	0.0396	-25.80
75.70	23.07	0	2	1.5		
75.71	23.08	0	1.5	1		
76.70	23.38	0	2	1		
76.71	23.38	0	1	2		
80.00	24.38	0	1.5	2		
80.01	24.39	0	1	1		
80.90	24.66	0	2	1		
80.91	24.66	0	1	1		
81.50	24.84	0	2	1		
81.51	24.84	0	1	1		
83.10	25.33	0	2	1		
83.11	25.33	0	2	1		
83.30	25.39	0	2	1	0.0523	-26.19
85.00	25.91	0	2	1		
85.01	25.91	0	2.5	1.5		
86.00	26.21	0	2.5	1.5		
86.01	26.22	0	1.5	1.5		
86.70	26.43	0	1.5	1.5		
86.71	26.43	0	1	2		
88.70	27.04	0	2	2		
88.71	27.04	0	1	1		
92.80	28.29	0	2	1		
92.81	28.29	0	1	1.5		
93.80	28.59	0	1	1.5	0.0605	-28.06
94.20	28.71	0	2	1.5		
94.21	28.72	0	1	1.5		
95.80	29.20	0	2	1.5		
95.81	29.20	0	1	2		
97.00	29.57	1	2	2	0.2017	-25.68
98.00	29.87	1	3	2		
98.01	29.87	0	1.5	1		
98.40	29.99	0	1.5	1		
98.41	30.00	0	1	2		
98.95	30.16	0	1	1.5	0.1622	-24.45
99.00	30.18	2	1	1.5		
99.01	30.18	1	3.5	1.5		

1. Silver Ridge B-1 Core

depth ft	depth m	color	grain size	depth rank	TOC %	δ13C
99.90	30.45	1	3.5	1.5		
99.91	30.45	0	1	1		
100.30	30.57	0	1	1		
100.31	30.57	1	3	1.5		
102.00	31.09	1	3	1.5		
102.01	31.09	0	1.25	2		
103.90	31.67	0	1.25	2		
103.91	31.67	0.5	2	2		
104.30	31.79	0.5	2	2		
104.31	31.79	0.5	1	1		
106.00	32.31	0.5	2	1		
106.01	32.31	0.5	1	2		
107.79	32.85	1.5	1.25	2	0.2564	-25.39
108.00	32.92	1.5	1.5	2		
108.01	32.92	1.5	2	2		
109.40	33.35	2	3	2		
109.41	33.35	2	3	1.5		
111.63	34.02	2	3	2	0.5288	-24.54
112.70	34.35	2	3	2		
112.71	34.35	2	2.5	2.5		
113.60	34.63	2	2.5	2.5		
113.61	34.63	2.5	2.5	3		
113.85	34.70	2.5	2	3	1.1276	-24.32
115.23	35.12	3	1	3	3.3571	-27.03
116.00	35.36	3	1	3		
116.01	35.36	2.5	2.5	3		
116.50	35.51	3	1	3		
116.51	35.51	2.5	1	3		
117.45	35.80	2.25	0.75	2.5	1.7755	-28.02
118.00	35.97	2	0.5	2.5		
118.01	35.97	2	0.5	2.5		
120.65	36.77	2	0.5	2.5	0.1756	-27.24
121.20	36.94	2	0.5	2.5		
121.21	36.94	2	1	1.5		
123.20	37.55	1.75	3	1.5		
123.21	37.55	2	1.5	1.5		
123.80	37.73	2	2	1.5	0.2139	-26.31
124.50	37.95	2	3	1.5		
124.51	37.95	1.5	1.5	1		
125.30	38.19	1.5	1.5	1		
125.31	38.19	2	1	1		

1. Silver Ridge B-1 Core

depth ft	depth m	color	grain size	depth rank	TOC %	δ13C
126.00	38.40	2	1	1		
126.01	38.41	1.5	2	1		
126.40	38.53	1.5	2	1		
126.41	38.53	2	1.5	0.5		
126.65	38.60	2	1.5	0.5	0.1770	-28.26
127.30	38.80	2	1.5	0.5		
127.31	38.80	2.25	2	1		
128.33	39.11	2.25	2	1	0.2628	-27.97
128.90	39.29	2.25	2	1		
128.91	39.29	2	2	1		
130.70	39.84	2	2	1		
130.71	39.84	2	4	1		
131.00	39.93	2	4	1		
131.01	39.93	2	4	1.5		
131.60	40.11	2	3.5	1.5		
131.61	40.11	2	1.5	1.5		
132.80	40.48	2	3	1.5		
132.81	40.48	2.5	1.5	2		
133.20	40.60	2.5	1.5	2	0.2542	-24.79
135.00	41.15	2.5	1.5	2		
135.01	41.15	2.75	1	2.5		
135.60	41.33	2.75	1	2.5	0.2693	-26.00
136.80	41.70	2.75	1	2.5		
136.81	41.70	2.75	1.5	2.5		
138.75	42.29	2.75	1.5	2.5	0.2712	-24.78
140.50	42.82	2.75	1.25	3		
140.51	42.83	2	2.5	2		
141.00	42.98	2	2.5	2	1.0605	-24.70
141.01	42.98	2.5	2	2		
141.70	43.19	2.5	2	2		
141.71	43.19	2.5	1.5	2		
141.90	43.25	2.5	1.5	2		
141.91	43.25	2.25	3	2		
142.20	43.34	2.25	3	2	0.3521	-27.11
142.60	43.46	2.25	3	2		
142.61	43.47	3	1	2.5		
143.20	43.65	2	2	2.5		
143.21	43.65	3	1	3		
143.53	43.75	3	1	3	2.4230	-28.01
143.80	43.83	3	1	3		
143.81	43.83	2	2	2.5		

1. Silver Ridge B-1 Core

depth ft	depth m	color	grain size	depth rank	TOC %	δ13C
143.90	43.86	2	2	2.5		
143.91	43.86	3	1	3		
144.40	44.01	3	1	3		
144.41	44.02	2	2	2.5		
144.50	44.04	2	2	2.5		
144.51	44.05	3	1	3		
145.26	44.28	3	0.8	3.5	3.7128	-28.08
145.90	44.47	3	0.75	4		
145.91	44.47	3	0.5	5		
146.00	44.50	3	0.5	5		
146.01	44.50	2	2	5		
146.10	44.53	2	2	5		
146.11	44.53	3	0.5	5		
146.25	44.58	3	0.5	5	2.7574	-27.07
146.80	44.74	3	0.5	5		
146.81	44.75	3	0.5	3		
150.90	45.99	2	0.5	3		
150.35	45.83	2.5	0.5	2.75	2.0021	-29.12
150.91	46.00	2	2	2.5		
152.95	46.62	2	3	2.25	0.2326	-25.85
155.60	47.43	2	4	2		
155.61	47.43	1.5	2	1.5		
156.87	47.81	1.5	2	1.5	0.1585	-27.68
158.70	48.37	1.5	2	1.5		
158.71	48.37	2	1	1.5		
159.33	48.56	2	1.5	1.5	0.1376	-24.75
160.40	48.89	1	2	1.5		
160.41	48.89	1	1.75	1		
162.10	49.41	0.75	3	1		
162.11	49.41	0.5	1.5	1		
162.45	49.51	0.5	1.5	1	0.1213	-26.14
164.90	50.26	0.5	1.5	1		
164.91	50.26	0.5	1.5	0.5		
166.10	50.63	0.5	1.5	0.5		
166.11	50.63	0.5	1.5	0.5		
166.70	50.81	0.5	1.5	1		
166.71	50.81	0.5	1.5	1		
169.70	51.72	0.5	1.5	0.6	0.1128	-24.04
170.00	51.82	0.5	1.5	0.5		
170.01	51.82	0.5	1.5	0.5		
171.00	52.12	2	1.5	2		

1. Silver Ridge B-1 Core

depth ft	depth m	color	grain size	depth rank	TOC %	δ13C
171.01	52.12	2	2	2.5		
171.25	52.20	2	2	2.5	0.1872	-26.16
172.50	52.58	2	2	2.5		
172.51	52.58	2	1.5	2.5		
174.65	53.23	2	1.5	2.5	3.0714	-25.54
175.00	53.34	2	1.5	2.5		
175.01	53.34	2.25	1.5	2.5		
175.50	53.49	2.25	1.5	2.75		
175.51	53.50	2	1.5	2		
177.00	53.95	2	1.5	2		
177.01	53.95	2	1	2.5		
177.15	54.00	2.2	1	2.5	0.4099	-26.37
178.00	54.25	2.5	1	2.5		
178.01	54.26	2	1.5	2.5		
178.50	54.41	2	1.5	2.5		
178.51	54.41	2.75	1	3		
180.25	54.94	2.85	1	3	1.9382	-28.86
181.00	55.17	3	1	3		
182.30	55.57	2.5	1	3.5		
182.31	55.57	3	0.75	4		
183.60	55.96	3	0.75	4	3.0333	-26.34
184.65	56.28	3	0.75	4	1.8791	-27.72
186.70	56.91	3	0.75	4	1.0205	-27.26
186.71	56.91	2	0.5	4		
186.90	56.97	2	0.5	4		
186.91	56.97	3	1.5	3		
190.10	57.94	3	1.5	2.75		
190.11	57.95	2	3	2.75		
192.22	58.59	2	3	2.6	0.1830	-24.12
195.00	59.44	2	3	2.1	3.4646	-25.35
196.10	59.77	2	3	2		
196.11	59.77	2	1	1.5		
197.31	60.14	2	2	1.5	0.1641	-27.30
198.20	60.41	1	3	1.5		
198.21	60.41	2	1	1		
199.70	60.87	2	3	1		
199.71	60.87	1.5	2	1		
201.40	61.39	1	4	1	0.3057	-27.88
201.41	61.39	1.5	1.5	1		
202.10	61.60	0.5	4.5	1		
202.11	61.60	1	2.75	1		

1. Silver Ridge B-1 Core

depth ft	depth m	color	grain size	depth rank	TOC %	δ13C
203.10	61.90	1	3	1		
203.11	61.91	2	2	1		
203.20	61.94	2	2.5	1	0.1808	-26.58
203.80	62.12	1	3	1		
203.81	62.12	0.75	1	0.75		
204.40	62.30	1	2	0.75		
204.41	62.30	0.5	1.25	1		
204.80	62.42	0.5	1.25	1		
204.81	62.43	0.5	1.5	1		
206.20	62.85	0.5	1.5	1		
206.21	62.85	1.5	4	1		
207.30	63.19	1.5	4	1	0.1114	-26.50
208.00	63.40	1.5	4	1		
208.01	63.40	0.25	1.5	1.5		
210.00	64.01	0.25	1.5	1.5		
210.01	64.01	1	1	1		
210.10	64.04	1	1	1	0.0951	-25.78
210.40	64.13	1	1	1		
210.41	64.13	0	1	1		
211.40	64.43	0	1	1		
211.41	64.44	1	1.5	2		
211.70	64.53	1	1.5	2		
211.71	64.53	2	3	1		
212.14	64.66	2	3	1	0.1202	-25.52
213.00	64.92	2	3	1		
213.01	64.93	0	1	2		
217.30	66.23	0.25	3	2		
217.31	66.24	0	1.5	1.5		
218.00	66.45	2	2	1.5		
218.01	66.45	2	2	1.5		
218.50	66.60	2	2	1.5	0.1564	-24.24
219.00	66.75	1	2.5	1.5		
219.01	66.75	1	1	2.5		
221.00	67.36	2	1	2.5		
221.01	67.36	2	1	2.75		
221.50	67.51	2	1	2.75	3.2111	-25.48
225.85	68.84	2	1	2.75	0.2353	-27.89
227.70	69.40	2	1	2.75		
227.71	69.41	0	1	1.5		
228.10	69.52	0	1	1.5		
228.11	69.53	2	1	2.75		

1. Silver Ridge B-1 Core

depth ft	depth m	color	grain size	depth rank	TOC %	δ13C
228.25	69.57	2	1	2.75	4.2342	-25.89
231.60	70.59	2	1	2.75	0.1118	-25.90
232.70	70.93	2	1	2.75		
232.71	70.93	2	2	3		
233.20	71.08	2	2	3		
233.21	71.08	2	1	3		
234.45	71.46	2.5	1.5	2.75	0.1289	-25.27
234.60	71.51	2	2	2.5		
234.61	71.51	2	3	2.5		
235.00	71.63	2	3	2.5		
235.01	71.63	2	1.5	2.5		
236.80	72.18	2	4	2.5		
236.81	72.18	2	1.5	2.5		
237.00	72.24	2	2	2.5	0.1431	-26.33
239.45	72.98	2	2.5	2.5	0.1457	-25.53
241.80	73.70	2	3	2.5		
241.81	73.70	2	1.5	3		
243.00	74.07	2	1.5	3	1.9185	-29.24
244.90	74.65	2	1.5	4		
244.91	74.65	2	1.25	3.5		
246.00	74.98	2.5	0.25	4		
246.01	74.98	2.5	0.25	4.5		
246.18	75.04	2.5	0.25	4.5	1.6382	-27.15
249.64	76.09	2.8	0.25	4.5	1.7275	-27.94
251.00	76.50	3	0.25	4.5		
251.01	76.51	3	0.25	4		
251.70	76.72	3	0.25	4		
251.71	76.72	3	0.25	4		
252.15	76.86	3	0.25	4	1.2002	-28.47
254.60	77.60	3	0.25	4		
254.61	77.61	3	1.5	4		
255.00	77.72	2.9	1.5	4	0.4646	-25.95
256.40	78.15	2.75	1.5	4		
256.41	78.15	2.75	1.5	3.5		
257.30	78.43	2.75	1.5	3.5		
257.31	78.43	2.75	1.5	3		
258.20	78.70	2	4	2.5		
258.21	78.70	2	3.5	1.5		
258.23	78.71	2	3.5	1.5	0.4396	-25.59
260.90	79.52	2	3.5	1.5	0.1351	-27.92
261.40	79.67	2	3.5	1.5		

1. Silver Ridge B-1 Core

depth ft	depth m	color	grain size	depth rank	TOC %	δ13C
261.41	79.68	2.5	3.5	1.5		
261.60	79.74	2.5	3	1.5		
261.61	79.74	2.5	3	1.5		
262.16	79.91	2.5	3	1.5	0.1061	-25.32
267.60	81.56	2.25	3.5	1.5	0.0942	-25.05
269.00	81.99	2	4	1.5		
269.01	81.99	2.25	3.5	1.5		
270.31	82.39	2.25	3.5	1.5	0.0840	-24.16
271.30	82.69	2.25	3.5	1.5	0.0853	-26.27
272.70	83.12	2.25	3.5	1.5		
272.71	83.12	2	3.5	1		
273.60	83.39	2	3.5	1		
273.61	83.40	2	2	2		
273.85	83.47	2	2	2	0.0915	-25.86
274.20	83.58	2	2	2		
274.21	83.58	2	4	1		
275.90	84.09	2	4	1		
275.91	84.10	2	4.25	1		
276.00	84.12	2	4.25	1		
276.01	84.13	2	4	1		
278.65	84.93	2	4	1	0.0935	-24.98
279.30	85.13	2	4	1		
279.31	85.13	2	4	1.5		
282.65	86.15	2	4	1.5	0.1184	-28.24
285.50	87.02	2	4	1.25	0.0615	-26.12
291.56	88.87	2	4	1.25	0.0613	-28.41
294.60	89.79	1.5	3.5	1		
294.61	89.80	1	4	1		
295.30	90.01	1	4	1		
295.31	90.01	0.5	4	1		
298.25	90.91	0.5	4	1	0.0568	-25.69
309.95	94.47	0.5	4	1	0.0406	-26.62
311.00	94.79	0.5	4	1		
311.01	94.80	0.5	4	1		
311.90	95.07	0.5	4	1		
311.91	95.07	0.25	4	1		
312.50	95.25	0.25	4	1		
312.51	95.25	0.5	4	1		
313.20	95.46	0.5	4	1		
313.21	95.47	0.5	2.5	1.5		
314.50	95.86	0.5	2.5	1		

1. Silver Ridge B-1 Core

depth ft	depth m	color	grain size	depth rank	TOC %	δ13C
314.51	95.86	0.5	4	1		
320.50	97.69	0.5	4	1		
320.51	97.69	0.25	1.5	1.5		
320.70	97.75	0.25	1.5	1		
320.71	97.75	0.5	4	1.5		
320.80	97.78	0.5	4	1.5	0.0603	-23.81
321.90	98.12	0.5	4	1		
321.91	98.12	0.5	1.5	1.5		
322.20	98.21	0.5	1.5	1		
322.21	98.21	0.5	3	0.5		
322.50	98.30	0.5	3	0.5		
322.51	98.30	0.5	1.5	0.5		
322.55	98.31	0.5	1.5	0.5	0.1096	-25.56
322.70	98.36	0.5	1.5	1		
322.71	98.36	0.5	4	1		
328.70	100.19	0.5	4	1		
328.71	100.19	0.25	2	1		
329.30	100.37	0.25	2	1		
329.31	100.37	0.25	3.5	1		
333.60	101.68	0.25	3.5	0.5		
333.61	101.68	0	2	0.5		
334.00	101.80	0	2	0.5		-25.05
335.80	102.35	0	2	1		
335.81	102.35	0.25	3.5	1		
339.00	103.33	0.25	3.5	1		
339.01	103.33	0.25	4	1		
341.00	103.94	0.25	4	1		
341.01	103.94	0.25	4	1		
348.50	106.22	0.25	4.5	1		
348.51	106.23	0.25	4	1		
349.30	106.47	0.25	6	1		
349.31	106.47	0.25	5	1		
350.00	106.68	0.25	6	1		
350.01	106.68	0.25	5	1		
352.20	107.35	0.25	6	1		
352.21	107.35	0.25	5	1		
353.20	107.66	0.25	6	1		
353.21	107.66	0.25	5	1		
355.80	108.45	0.25	7	1		
355.81	108.45	0.25	5	1		
356.70	108.72	0.25	6	1		

1. Silver Ridge B-1 Core

depth ft	depth m	color	grain size	depth rank	TOC %	δ13C
356.71	108.73	0.25	3.5	1		
356.80	108.75	0.25	3.5	1		
356.81	108.76	0.25	5	1		
357.50	108.97	0.25	6	1		
357.51	108.97	0.25	5	1		
358.40	109.24	0.25	6	1		
358.41	109.24	0.25	5	1		
359.50	109.58	0.25	6	1		
359.51	109.58	0.25	5	1		
362.00	110.34	0.25	9	1		
362.01	110.34	0.25	4.5	1		
363.00	110.64	0.25	5	1		
363.01	110.65	0.25	4.5	1		
363.40	110.76	0.25	5	1		
363.41	110.77	0.25	4	1		
364.00	110.95	0.25	5	1		
364.01	110.95	0.25	8	1		
365.10	111.28	0.25	6	1		
365.11	111.29	0.25	3.5	1		
365.50	111.40	0.25	3.5	1		
365.51	111.41	0.25	7	1		
366.30	111.65	0.25	7	1		
366.31	111.65	0.25	4	1		
366.40	111.68	0.25	4	1		
366.41	111.68	0.25	5	1		
367.60	112.04	0.25	6	1		
367.61	112.05	0.25	3	1		
368.70	112.38	0.25	6	1		
368.71	112.38	0.25	4	1		
370.00	112.78	0.25	8	1		
370.01	112.78	0.25	7	1		
371.00	113.08	0.25	7	1		

Appendix A
2. n-alcane data from Silver Ridge B1

NC 25	NC 26	NC 27	NC 28	NC 29	NC 30	NC 31	Weighted Mean	Mean	Weighted Mean Odd	CPI	ACL
Silver Ridge B-1-138.75											
-29.83	-30.08	-30.42	-30.61	-30.44	-30.97	-30.93	-30.50	-30.47	-30.44	1.0	28.2
Silver Ridge B1_146.25											
-29.46	-29.64	-30.13	-30.04	-29.93	-30.62	-30.85	-29.95	-30.09	-29.93	1.1	27.2

3. Bluff Head Fish and d13C data

cm from base	Huber column	cornet chart column	cops	semi	redf	ptych	cops/ cm	sem/ cm	redf/ cm	ptych/ cm	moles C	% C	δ13C	δ15N
0.00	1, 4	none	0	0	0	0	0.00	0.00	0.00	0.00	1.4090E-05	2.39	-26.9810	1.8780
2.00	1, 4	none	0	0	0	0	0.00	0.00	0.00	0.00	1.4090E-05	2.39	-26.9810	1.8780
2.01	3	none	0	0	0	0	0.00	0.00	0.00	0.00	1.2780E-05	2.49	-27.8358	-7.3031
6.70	3	none	0	0	0	0	0.00	0.00	0.00	0.00	1.2780E-05	2.49	-27.8358	-7.3031
6.71	2, 7	none	0	0	0	0	0.00	0.00	0.00	0.00	2.2970E-05	4.60	-28.4261	3.7752
9.90	2, 7	none	0	0	0	0	0.00	0.00	0.00	0.00	2.2970E-05	4.60	-28.4261	3.7752
9.91	gap	none	0	0	0	0	0.00	0.00	0.00	0.00				
11.20	gap	none	0	0	0	0	0.00	0.00	0.00	0.00				
11.21	6	22AB	0.5	1	1	0	1.00	2.00	2.00	0.00	5.2790E-05	10.74	-27.1294	6.6860
11.70	6	22AB	0.5	1	1	0	1.00	2.00	2.00	0.00	5.2790E-05	10.74	-27.1294	6.6860
11.71	8	22AB_2.2, 3.1	4.5	2	4	0	3.00	1.33	2.67	0.00	2.5820E-05	5.16	-26.9588	1.1135
13.20	8	22AB_2.2, 3.1	4.5	2	4	0	3.00	1.33	2.67	0.00	2.5820E-05	5.16	-26.9588	1.1135
13.21	9	22AB_1, 2.1, 2.2	12	4	10	0	3.16	1.05	2.63	0.00	1.6460E-05	3.31	-27.3725	-1.0283
17.00	9	22AB_1, 2.1, 2.2	12	4	10	0	3.16	1.05	2.63	0.00	1.6460E-05	3.31	-27.3725	-1.0283
17.01	9	21AB_4	0	0	0	0	0.00	0.00	0.00	0.00	1.6460E-05	3.31	-27.3725	-1.0283
18.30	9	21AB_4	0	0	0	0	0.00	0.00	0.00	0.00	1.6460E-05	3.31	-27.3725	-1.0283
18.31	gap	21AB_2, 3	3	1	1	1	0.81	0.27	0.27	0.27				
22.00	gap	21AB_2, 3	3	1	1	1	0.81	0.27	0.27	0.27				
22.01	10	21AB_1	0	2	2	0	0.00	2.50	2.50	0.00	2.4620E-05	5.09	-27.6013	0.7782
22.80	10	21AB_1	0	2	2	0	0.00	2.50	2.50	0.00	2.4620E-05	5.09	-27.6013	0.7782
22.81	11	20AB3	1	3	5	1	0.83	2.50	4.17	0.83	3.5320E-05	7.17	-27.1502	3.9459
24.00	11	20AB3	1	3	5	1	0.83	2.50	4.17	0.83	3.5320E-05	7.17	-27.1502	3.9459
24.01	12	20AB2	0	1	4	1	0.00	0.67	2.67	0.67	3.6800E-05	7.52	-27.3694	3.7672
25.50	12	20AB2	0	1	4	1	0.00	0.67	2.67	0.67	3.6800E-05	7.52	-27.3694	3.7672
25.51	gap	20AB1	0	0	3	1	0.00	0.00	2.14	0.71				
26.90	gap	20AB1	0	0	3	1	0.00	0.00	2.14	0.71				
26.91	13	19AB	1	0	8	0	0.38	0.00	3.08	0.00	2.5330E-05	5.00	-27.0459	1.2858
29.50	13	19AB	1	0	8	0	0.38	0.00	3.08	0.00	2.5330E-05	5.00	-27.0459	1.2858
29.51	14	18AB	1	0	2	0	2.00	0.00	4.00	0.00	2.4860E-05	5.06	-27.1443	3.0526
30.00	14	18AB	1	0	2	0	2.00	0.00	4.00	0.00	2.4860E-05	5.06	-27.1443	3.0526

3. Bluff Head Fish and d13C data

cm from base	Huber column	cornet chart column	cops	semi	redf	ptych	cops/ cm	sem/ cm	redf/ cm	ptych/ cm	moles C	% C	δ13C	δ15N
30.01	15	18AB	3	0	6	0	1.50	0.00	3.00	0.00	2.7060E-05	5.45	-27.1230	2.2229
32.00	15	18AB	3	0	6	0	1.50	0.00	3.00	0.00	2.7060E-05	5.45	-27.1230	2.2229
32.01	18	17AB	1	0	5	1	1.11	0.00	5.56	1.11	3.3220E-05	6.51	-27.1896	2.2259
32.90	18	17AB	1	0	5	1	1.11	0.00	5.56	1.11	3.3220E-05	6.51	-27.1896	2.2259
32.91	18	16AB bottom	0.7	0	4	0	0.44	0.00	2.50	0.00	3.3220E-05	6.51	-27.1896	2.2259
34.50	18	16AB bottom	0.7	0	4	0	0.44	0.00	2.50	0.00	3.3220E-05	6.51	-27.1896	2.2259
34.51	17	16AB top	0.3	0	2	0	0.12	0.00	0.80	0.00	3.0260E-05	5.98	-27.1686	3.9657
37.00	17	16AB top	0.3	0	2	0	0.12	0.00	0.80	0.00	3.0260E-05	5.98	-27.1686	3.9657
37.01	gap	15AB,14AB bottom	2.5	0	3.5	0.5	2.50	0.00	3.50	0.50				
38.00	gap	15AB,14AB bottom	2.5	0	3.5	0.5	2.50	0.00	3.50	0.50				
38.01	19	14AB top	2.5	0	3.5	0.5	3.13	0.00	4.38	0.63	3.0550E-05	5.97	-27.1786	5.1429
38.80	19	14AB top	2.5	0	3.5	0.5	3.13	0.00	4.38	0.63	3.0550E-05	5.97	-27.1786	5.1429
38.81	20	13AB	2	0	6.5	0	1.43	0.00	4.64	0.00	2.8120E-05	5.61	-26.9841	-0.7041
40.20	20	13AB	2	0	6.5	0	1.43	0.00	4.64	0.00	2.8120E-05	5.61	-26.9841	-0.7041
40.21	21	12AB - 9AB2	5.5	0	26	0.5	3.06	0.00	14.44	0.28	2.5650E-05	4.98	-26.7514	2.1072
42.00	21	12AB - 9AB2	5.5	0	26	0.5	3.06	0.00	14.44	0.28	2.5650E-05	4.98	-26.7514	2.1072
42.01	22	12AB - 9AB2	7	0.5	51	0.5	1.75	0.13	12.75	0.13	2.3760E-05	4.93	-26.7169	3.6715
46.00	22	12AB - 9AB2	7	0.5	51	0.5	1.75	0.13	12.75	0.13	2.3760E-05	4.93	-26.7169	3.6715
46.01	23	12AB - 9AB2	1	0.5	4.5	0	1.00	0.50	4.50	0.00	1.7110E-05	3.43	-26.7944	-4.8660
47.00	23	12AB - 9AB2	1	0.5	4.5	0	1.00	0.50	4.50	0.00	1.7110E-05	3.43	-26.7944	-4.8660
47.01	24	9AB1	1	0	14	1	0.67	0.00	9.33	0.67	1.8410E-05	3.73	-27.1865	5.4764
48.50	24	9AB1	1	0	14	1	0.67	0.00	9.33	0.67	1.8410E-05	3.73	-27.1865	5.4764
48.51	25	8AB3 - 8AB2	3	1	7	0	1.76	0.59	4.12	0.00	1.4870E-05	2.89	-26.7999	-2.6780
50.20	25	8AB3 - 8AB2	3	1	7	0	1.76	0.59	4.12	0.00	1.4870E-05	2.89	-26.7999	-2.6780
50.21	26	8AB1	0	0	0	0	0.00	0.00	0.00	0.00	2.0890E-05	4.18	-26.6844	1.4276
52.50	26	8AB1	0	0	0	0	0.00	0.00	0.00	0.00	2.0890E-05	4.18	-26.6844	1.4276
52.51	gap	7AB3 - 7AB2	0	10	0	0	0.00	6.67	0.00	0.00				
54.00	gap	7AB3 - 7AB2	0	10	0	0	0.00	6.67	0.00	0.00				
54.01	30, 27	7AB1 - 6AB1,2 - 5AB4	0	21	0	1	0.00	10.00	0.00	0.48	2.9180E-05	6.04	-27.5751	2.4844
56.10	30, 27	7AB1 - 6AB1,2 - 5AB4	0	21	0	1	0.00	10.00	0.00	0.48	2.9180E-05	6.04	-27.5751	2.4844

3. Bluff Head Fish and d13C data

cm from base	Huber column	cornet chart column	cops	semi	redf	ptych	cops/ cm	sem/ cm	redf/ cm	ptych/ cm	moles C	% C	δ13C	δ15N
56.11	29, 28	5AB3 - 5AB2	0	37	0	2	0.00	16.82	0.00	0.91	1.7630E-05	3.46	-27.4908	4.5983
58.30	29, 28	5AB3 - 5AB2	0	37	0	2	0.00	16.82	0.00	0.91	1.7630E-05	3.46	-27.4908	4.5983
58.31	gap	5AB1	0	15	0	2	0.00	75.00	0.00	10.00				
58.50	gap	5AB1	0	15	0	2	0.00	75.00	0.00	10.00				
58.51	gap	4AB6	0	1	0	0	0.00	0.42	0.00	0.00				
60.90	gap	4AB6	0	1	0	0	0.00	0.42	0.00	0.00				
60.91	gap	4AB5 = 4AB4_1	0	40	0	2	0.00	15.38	0.00	0.77				
63.50	gap	4AB5 = 4AB4_1	0	40	0	3	0.00	15.38	0.00	1.15				
63.51	gap	4AB5 = 4AB4_2	0	0	0	0	0.00	0.00	0.00	0.00				
64.40	gap	4AB5 = 4AB4_2	0	0	0	0	0.00	0.00	0.00	0.00				
64.41	31	4AB4 - 4AB4_1	1	33	0	1	0.91	30.00	0.00	0.91	1.2080E-05	2.46	-27.1391	4.1754
65.50	31	4AB4 - 4AB4_1	1	33	0	1	0.91	30.00	0.00	0.91	1.2080E-05	2.46	-27.1391	4.1754
65.51	32	4AB2 - 4AB3 - 4AB1_3	0	21	0	1	0.00	9.13	0.00	0.43	3.0290E-05	6.16	-27.2383	5.0499
67.80	32	4AB2 - 4AB3 - 4AB1_3	0	21	0	1	0.00	9.13	0.00	0.43	3.0290E-05	6.16	-27.2383	5.0499
67.81	33	3AB 4A4 - 4AB1_1 - 4AB1_2	0	5	0	0	0.00	1.85	0.00	0.00	3.7560E-05	7.77	-27.9128	3.6807
70.50	33	3AB 4A4 - 4AB1_1 - 4AB1_2	0	5	0	0	0.00	1.85	0.00	0.00	3.7560E-05	7.77	-27.9128	3.6807
70.51	gap	3B3 4A3 - 4A2	0	2	0	0	0.00	1.00	0.00	0.00				
72.50	gap	3B3 4A3 - 4A3	0	2	0	0	0.00	1.00	0.00	0.00				
72.51	34	3B2b - 3B2t	0	14	0	0	0.00	5.00	0.00	0.00	4.1130E-05	8.23	-28.1006	-3.6221
75.30	34	3B2b - 3B2t	0	14	0	0	0.00	5.00	0.00	0.00	4.1130E-05	8.23	-28.1006	-3.6221
75.31	35	3B1	0	16	0	0	0.00	7.27	0.00	0.00	1.0500E-05	2.14	-27.8239	-7.6543
77.50	35	3B1	0	16	0	0	0.00	7.27	0.00	0.00	1.0500E-05	2.14	-27.8239	-7.6543
77.51	36	2B	0	0	0	0	0.00	0.00	0.00	0.00	2.6620E-05	5.50	-27.9969	3.3989
78.70	36	2B	0	0	0	0	0.00	0.00	0.00	0.00	2.6620E-05	5.50	-27.9969	3.3989
78.71	37	2B	0	0	0	0	0.00	0.00	0.00	0.00	1.5180E-05	2.97	-27.9001	3.1616
80.00	37	2B	0	0	0	0	0.00	0.00	0.00	0.00	1.5180E-05	2.97	-27.9001	3.1616
80.01	38	1B	0	0	0	0	0.00	0.00	0.00	0.00	1.4550E-05	3.00		
81.30	38	1B	0	0	0	0	0.00	0.00	0.00	0.00	1.4550E-05	3.00		
81.31	gap	2A1A top	0	1	0	0	0.00	0.31	0.00	0.00				
84.50	gap	2A1A top	0	1	0	0	0.00	0.31	0.00	0.00				

3. Bluff Head Fish and d13C data

cm from base	Huber column	cornet chart column	cops	semi	redf	ptych	cops/ cm	sem/ cm	redf/ cm	ptych/ cm	moles C	% C	δ13C	δ15N
84.51	39	1A	0	0	0	0	0.00	0.00	0.00	0.00	1.2630E-05			
86.50	39	1A	0	0	0	0	0.00	0.00	0.00	0.00	1.2630E-05			
86.51	40	none	0	0	0	0	0.00	0.00	0.00	0.00	4.2680E-06			
89.50	40	none	0	0	0	0	0.00	0.00	0.00	0.00	4.2680E-06			
89.51	41	none	0	0	0	0	0.00	0.00	0.00	0.00	1.0940E-05	2.13	-28.3406	3.6404
91.00	41	none	0	0	0	0	0.00	0.00	0.00	0.00	1.0940E-05	2.13	-28.3406	3.6404
91.01	42	none	0	0	0	0	0.00	0.00	0.00	0.00	2.5720E-06			-2.0827
95.80	42	none	0	0	0	0	0.00	0.00	0.00	0.00	2.5720E-06			-2.0827
95.81	43	sandstone	0	0	0	0	0.00	0.00	0.00	0.00	2.3920E-05			
104.50	43	sandstone	0	0	0	0	0.00	0.00	0.00	0.00	2.3920E-05			
104.51	44	sandstone	0	0	0	0	0.00	0.00	0.00	0.00	7.6910E-06	1.74	-28.3591	2.7864
107.50	44	sandstone	0	0	0	0	0.00	0.00	0.00	0.00	7.6910E-06	1.74	-28.3591	2.7864
107.51	45	sandstone	0	0	0	0	0.00	0.00	0.00	0.00	1.4010E-06			-7.1660
114.50	45	sandstone	0	0	0	0	0.00	0.00	0.00	0.00	1.4010E-06			-7.1660

Notes

1. Carbon Preference Index (CPI) and Average Chain Length (ACL) for A.2.

Carbon Preference Index (CPI) was calculated using a modified version of the "improved" (CPI2) method of Marzi et al. (1993) using the following formula:

$$½([(A_{25} + A_{27} + A_{29})/(A_{26} + A_{28} + A_{30})] + [(A_{27} + A_{29} + A_{31})/(A_{26} + A_{28} + A_{30})]) \quad (1)$$

Average Chain Length (ACL) was calculated using a formula modified from Smith et al. (2008) as follows:

$$ACL= [(25*A_{25})+ (27*A_{27}) + (29*A_{29}) + (31*A_{31})] / (A_{25} + A_{27} + A_{29} + A_{31}) \quad (2)$$

In both equations 1 and 2, A is the area under the chromatographic peak for each n-alkane of a specific chain length and for equation 2, 25, 27, 29, 31 are the individual n-alkane chain lengths.